This is a preprint, the final version is subject to change, of the American Mineralogist (MSA)
Cite as Authors (Year) Title. American Mineralogist, in press.
(DOI will not work until issue is live.) DOI: http://dx.doi.org/10.2138/am.2013.4364

Effect of particle size on phase transitions in metastable alumina nanoparticles: A view from high-resolution solid-state ^{27}Al NMR study

Kim, Hyun Na[1] and Lee, Sung Keun[1,*]

School of Earth and Environmental Sciences

Seoul National University

Seoul, 151-742 Korea

*Corresponding author,

Lee, Sung Keun

Associate Professor

School of Earth and Environmental Sciences,

Seoul National University, Seoul, 151-742, Republic of Korea

E-mail: sungklee@snu.ac.kr

Web: http://plaza.snu.ac.kr/~sungklee

Revised version submitted to "American Mineralogist (MS# 4364)"

2-5-2013

This is a preprint, the final version is subject to change, of the American Mineralogist (MSA)
Cite as Authors (Year) Title. American Mineralogist, in press.
(DOI will not work until issue is live.) DOI: http://dx.doi.org/10.2138/am.2013.4364

Abstract

Detailed knowledge of the atomic structures of diverse metastable/stable polymorphs in alumina nanoparticles with varying particle size is essential to understand their macroscopic properties and their phase transition behaviors. In this study, we report high-resolution solid-state ^{27}Al 2D triple-quantum (3Q) magic-angle spinning (MAS) and 1D MAS nuclear magnetic resonance (NMR) spectra for alumina nanoparticles with varying temperature and particle size with an aim to explore the nature of phase transitions in alumina nanoparticles. Although the ^{27}Al MAS NMR spectra of alumina nanoparticles cannot fully resolve all the crystallographically distinct Al sites for metastable aluminas such as γ-, δ-, and θ-Al_2O_3, the simulation of ^{27}Al MAS NMR spectra collected at different magnetic fields following the Czjzek model allows us to obtain the quantitative fractions of alumina polymorphs in nanoparticles and the NMR characteristics of their Al sites. The ^{27}Al 3QMAS NMR spectra resolved crystallographically distinct $^{[6]}$Al and $^{[4]}$Al sites in (γ, δ)- and θ-Al_2O_3 in the isotropic dimension for the first time. The fraction of θ-Al_2O_3 gradually increases up to ~1473 K at the expense of a decrease in (γ, δ)-Al_2O_3. The onset of formation of α-Al_2O_3 from metastable aluminas is observed above ~1493 K. Several phase transitions in alumina nanoparticles observed in the current study include, γ, δ → θ-Al_2O_3, γ, δ → α-Al_2O_3, and θ → α-Al_2O_3. Although the phase transition γ, δ → θ-Al_2O_3 occurs gradually with increasing annealing temperature from 873 K to 1473 K, the phase transitions γ, δ → α-Al_2O_3 and θ → α-Al_2O_3 occur dramatically within a narrow temperature range between 1473 K and 1573 K. The observed difference in temperature range (gradual *vs.* dramatic) for phase transition γ, δ → θ-Al_2O_3 and γ, δ, θ → α-Al_2O_3 originates from the different structural disorder in the metastable aluminas (i.e., γ-, δ-, θ-) and α-Al_2O_3. The effect of particle size on the phase transition (γ, δ) → θ-Al_2O_3 between 298 K and ~1473 K is not observed significantly. On the other hand, the transition temperature for γ, δ, θ → α-Al_2O_3, where the 50 % for alumina is α-Al_2O_3, apparently

This is a preprint, the final version is subject to change, of the American Mineralogist (MSA)
Cite as Authors (Year) Title. American Mineralogist, in press.
(DOI will not work until issue is live.) DOI: http://dx.doi.org/10.2138/am.2013.4364 7/11

increases as the particle size increases (as evidenced by TEM observation), indicating a larger energy penalty for phase transitions into α-Al_2O_3 in larger alumina nanoparticles. This could be due to higher surface energy of θ-Al_2O_3 than that of α-Al_2O_3 and/or the fact that transition from θ-Al_2O_3 to α-Al_2O_3 is kinetically favored for smaller nanoparticles. The mechanistic details of phase transitions among alumina polymorphs provided in the current study yield insights into the nature of the phase transition mechanisms for other oxide nanoparticles ubiquitous in the earth's surface environment.

1. Introduction

The atomic structure of alumina and the phase transition mechanism have long been investigated in many experimental and theoretical studies due to its fundamental interest as one of the simplest covalent oxides (Fitzgerald et al., 1997; Gan et al., 2009; Hagaman et al., 2010; John et al., 1983; Kryukova et al., 2000; Levin and Brandon, 1998; MacKenzie and Smith, 2002; O'Dell et al., 2007; Ollivier et al., 1997; Perander et al., 2007; Pinto et al., 2004; Repelin and Husson, 1990). Alumina also has diverse industrial uses, for example, in catalysts, adsorbents, and gate microelectronic devices (e.g., Kresse et al., 2005). Given these important roles of alumina, the atomic structures of diverse alumina polymorphs are relatively well known (Levin and Brandon, 1998 and references therein). However, the nature of phase transitions among alumina polymorphs is not fully understood due to manifested configurational disorder and their pronounced metastability (see below for further discussion), which leads to broad ranges of transition temperatures rather than a single well-defined transition temperature between polymorphs. Additionally, the effect of particle size on phase transitions among metastable phases in nanoparticles has not been fully investigated. Because the large surface area of nanoparticles plays an essential role in controlling their phase transition behaviors, it is necessary to explore the effect of particle size on the transition

This is a preprint, the final version is subject to change, of the American Mineralogist (MSA)
Cite as Authors (Year) Title. American Mineralogist, in press.
(DOI will not work until issue is live.) DOI: http://dx.doi.org/10.2138/am.2013.4364 7/11

temperature of alumina nanoparticles. The objective of this study is to investigate the effect of particle size on the nature of phase transitions among alumina polymorphs including metastable phases in alumina nanoparticles.

In addition to the well-known stable α-Al_2O_3 with a corundum structure, diverse metastable polymorphs have also been reported. These include γ-, δ-, θ-, κ-, χ-, and η-Al_2O_3, and are often called metastable aluminas with their stability fields depending on the annealing temperature, time, and types of precursor (Levin and Brandon, 1998 and references therein). For instance, γ-AlOOH (i.e., boehmite) transforms to α-Al_2O_3 via γ-, δ-, and θ-Al_2O_3. The transition temperatures between γ- and δ-Al_2O_3, between δ- and θ-Al_2O_3, and between θ- and α -Al_2O_3 are ~ 700–800, 900–1000, and 1000–1100°C, respectively (Levin and Brandon, 1998; Santos and Santos, 1992 and references therein). Extensive studies of temperature-induced phase transitions of alumina have revealed that the temperature of the transition from metastable alumina such as γ- and θ-Al_2O_3 into stable α-Al_2O_3 varied with the particle size (Bokhimi et al., 2001; Gan et al., 2009), defects density (Liu et al., 2005), and presence of seeds (Nordahl and Messing, 2002; Rajendran, 1994).

In particular, the particle size (i.e., surface area) of alumina nanoparticles has been identified as one of the crucial factors controlling the relative stability of γ-Al_2O_3 and its phase transitions (McHale et al., 1997a; Navrotsky, 2001). The effect of particle size on the nature of the phase transitions among alumina polymorphs is due to an increased role of the surface energy with decreasing particle size (e.g., Navrotsky, 2001). An alumina polymorph with lower surface energy becomes more stable than one with higher surface energy as the particle size decreases (i.e., the surface area increases). A molecular dynamics simulation demonstrated that surface energy of α-Al_2O_3 is larger than that of γ-Al_2O_3, which is consistent with calorimetric data for nanocrystalline alumina (Blonski and Garofalini, 1993; McHale et al., 1997b). Additional differential thermal analysis for phase transition from boehmite into α-

This is a preprint, the final version is subject to change, of the American Mineralogist (MSA)
Cite as Authors (Year) Title. American Mineralogist, in press.
(DOI will not work until issue is live.) DOI: http://dx.doi.org/10.2138/am.2013.4364 7/11

Al_2O_3 showed that transition temperature for $\gamma \rightarrow \alpha$-$Al_2O_3$ decreases from 1565 K to 1465 K as the crystallite size of boehmite decreases (Bokhimi et al., 2001). The systematic, spectroscopic study of the effect of particle size of γ-Al_2O_3 nanoparticles and other alumina polymorphs remains to be explored.

The atomic structure and phase transitions of alumina polymorphs have been studied mainly using X-ray diffraction (XRD), transmission electron microscopy (TEM), and solid-state nuclear magnetic resonance (NMR) spectroscopy. XRD and TEM studies have successfully provided the atomic structure of crystalline alumina of the γ-, θ-, and α-Al_2O_3, (Figure 1). These studies using TEM and XRD studies have furthered our understanding of the atomic structure and phase transition mechanism of metastable aluminas (Gan et al., 2009; Levin et al., 1997; Lin et al., 2004; Macedo et al., 2007; Ollivier et al., 1997; Yang et al., 1988). Its application to heterogeneous metastable aluminas can, however, be limited because the XRD patterns for those alumina phases are not well distinguished due to low crystallinity and significant degree of disorder in the metastable aluminas, (e.g., γ- and δ-Al_2O_3). Furthermore, because the temperature ranges of stability of each metastable alumina overlap, two or more phases can coexist in a sample within a given temperature range. It is often difficult to obtain the quantitative fractions of alumina polymorphs using either XRD or TEM (Levin et al., 1997; Ollivier et al., 1997; Yang et al., 1988).

NMR spectroscopy providing short-range structures around a specific nuclide of interest has been particularly effective in exploring the atomic structure of disordered oxide materials. Previous ^{27}Al magic-angle spinning (MAS) NMR studies have provided the atomic configuration of oxygen and aluminum atoms in crystalline alumina (Fitzgerald et al., 1997; John et al., 1983; MacKenzie and Smith, 2002; Mastikhin et al., 1981; O'Dell et al., 2007; Piedra et al., 1996) as well as amorphous alumina thin films (Lee et al., 2009b; Lee et al., 2010b). The atomic scale structure of quadrupolar nuclei (e.g., ^{27}Al) in alumina can be described by

This is a preprint, the final version is subject to change, of the American Mineralogist (MSA)
Cite as Authors (Year) Title. American Mineralogist, in press.
(DOI will not work until issue is live.) DOI: http://dx.doi.org/10.2138/am.2013.4364

129 structurally relevant NMR parameters such as the quadrupolar coupling constant (C_q),
130 asymmetry parameter (η), and isotropic chemical shift (δ_{iso}). Simulation of the 1D MAS NMR
131 spectra with these NMR parameters allows us to obtain the quantitative fraction of each phase
132 in a sample with heterogeneous mixtures of multiple phases (as is the case for the current
133 nanoparticles) (Ashbrook and Duer, 2006; Ashbrook and Smith, 2006; Duer, 2004; Lee and
134 Stebbins, 2003; Lee et al., 2003; Lee and Weiss, 2008; Phillips, 2000). To confirm the NMR
135 characteristics of Al sites in alumina polymorphs, previous ^{27}Al NMR studies of alumina have
136 analyzed the spinning sideband and simultaneously simulated ^{27}Al MAS NMR spectra θ- and
137 α-Al_2O_3 collected at different magnetic fields (O'Dell et al., 2007; Pecharroman et al., 1999;
138 Perander et al., 2007; Sabarinathan et al., 2010). The analysis of spinning sideband patterns in
139 ^{27}Al MAS NMR spectra has yielded excellent results and confirmed the NMR parameters of Al
140 sites in α-Al_2O_3 (Pecharroman et al., 1999; Sabarinathan et al., 2010). A simulation of the central
141 transition peak in ^{27}Al MAS NMR spectra measured at different magnetic fields (e.g., 8.4 T and
142 14.1 T) also successfully obtained the NMR parameters for Al sites in θ-Al_2O_3 (O'Dell et al.,
143 2007). A recent study also reported the simulation of ^{27}Al MAS NMR spectra for γ-Al_2O_3 using
144 the Czjzek model that have been effective in resolving Al sites in the disordered oxides (de
145 Lacaillerie et al., 2008; Lee et al., 2009a; Massiot et al., 2002; Neuville et al., 2004).

146 Recent progress in 2D triple-quantum (3Q) MAS also provide much improved
147 resolution among the different sites for quadrupolar nuclides (e.g., ^{27}Al, ^{17}O) (Lee, 2005; Lee et
148 al., 2010a; Massiot et al., 1996; Neuville et al., 2004; Stebbins et al., 2000; Stebbins et al., 1999;
149 Tangeman et al., 2004; Xue et al., 2010). ^{27}Al 3QMAS NMR method has been used to elucidate
150 the atomic scale structures of a single phase of crystalline and amorphous alumina (e.g., γ-
151 Al_2O_3 or α-Al_2O_3) as well as aluminum (oxy)hydroxides (e.g., boehmite, bayerite, gibbsite)
152 (Chupas et al., 2001; Damodaran et al., 2002; Hagaman et al., 2010; Lee et al., 2009b; Lee et al.,
153 2010b), and thus it may also be useful to resolve crystallographically distinct Al sites in

This is a preprint, the final version is subject to change, of the American Mineralogist (MSA)
Cite as Authors (Year) Title. American Mineralogist, in press.
(DOI will not work until issue is live.) DOI: http://dx.doi.org/10.2138/am.2013.4364 7/11

multiple phases of alumina with varying temperature.

Here, we explore the atomic structure of alumina polymorphs and the effect of particle size on the nature of phase transitions in alumina nanoparticles using high-resolution solid-state NMR. The NMR characteristics as well as fractions of Al sites in metastable aluminas are obtained by simulating ^{27}Al MAS NMR spectra measured at different magnetic fields. We also report the first ^{27}Al 3QMAS NMR spectra of resolved alumina nanoparticles resolving alumina polymorphs including (γ, δ)-, θ- and α-Al_2O_3. On the basis of the data from these NMR results, we provide an improved insight into the nature of phase transitions of alumina nanoparticles with emphasis on the effect of particle size.

2. Experimental Methods

2.1. Sample Preparation and Characterization

Three types of alumina nanoparticles, FA51, FA81, and FA100 (Cabot Co., SpectAl series) with surface areas of 55±10, 79±10, and 97±19 m^2/g, respectively, were used. The particle sizes (i.e., diameters) of the alumina nanoparticles calculated using a spherical approximation ($d = 6/S_0\rho$, where d is the average particle size, S_0 is the specific surface area, and ρ is the true density of the material) are 27, 19, and 15 nm for FA51, FA81, and FA100, respectively. Here, we refer to FA51, FA81, and FA100 as 27, 19, and 15 nm alumina nanoparticles, respectively. The alumina nanoparticles were heated for 2 h at temperatures ranging from 873 to 1473 K in a vertical tube furnace. As for standard metastable alumina, the crystalline γ-alumina was also purchased from Sigma Aldrich (product no. 544833).

2.2. X-ray Diffraction Spectroscopy and Transmission Electron Microscopy

The X-ray diffraction patterns were collected on New D8 Advance (Bruker) using Cu

This is a preprint, the final version is subject to change, of the American Mineralogist (MSA)
Cite as Authors (Year) Title. American Mineralogist, in press.
(DOI will not work until issue is live.) DOI: http://dx.doi.org/10.2138/am.2013.4364

K_α *X*-rays, a 2θ range of 15–75°, a step width of 0.02°, and a scan rate of 1°/min. The transmission electron microscopy (TEM) study was performed on a 300 kV JEM-2100 instrument (JEOL Ltd.) with a Gatan digital camera. The specimens for electron microscopy were prepared by suspending them in ethanol and placing a few droplets of the suspension on a carbon-coated film.

2.3. ^{27}Al NMR Spectroscopy

^{27}Al MAS spectra were collected at various magnetic fields on Varian 400 MHz (9.4 T), Bruker 500 MHz (11.7 T), and Varian 600 MHz (14.1 T) spectrometers with a triple resonance 4 mm Bruker probe, 4 mm Doty Scientific MAS probe, and 2.5 mm Varian probe, respectively. Single-pulse acquisition with a pulse length of 0.2 μs [radio frequency tip angle of about 15° for solids] was used with a recycle delay of 1 s and spinning speeds of 15 kHz at 9.4 and 11.7 T and 20 kHz at 14.1 T. The simulation of ^{27}Al MAS spectra was performed with the Dmfit program (Massiot et al., 2002). ^{27}Al 3QMAS NMR spectra were collected on the Varian 400 MHz (9.4 T) spectrometer using a fast amplitude modulation- (FAM-) based shifted-echo pulse sequences (1 s relaxation delay–3.0 μs pulse for 3Q excitation–t_1 delay–FAM pulse train with a 0.6 μs pulse-echo delay–15 μs soft pulse for echo reconversion–t_2 acquisition) with a spinning speed of 15 kHz (Kentgens and Verhagen, 1999; Madhu et al., 1999). An $AlCl_3$ solution of 2 mol% was used as an external frequency standard.

3. Results and Discussion

3.1. Characterization of Alumina Nanoparticles

Figure 2 shows TEM images of alumina nanoparticles of several sizes with increasing annealing temperature. The as-received alumina nanoparticles are mostly spherical and aggregated. Although the particle sizes varies (from ~16 to ~50 nm for FA51, from ~14 to ~26

This is a preprint, the final version is subject to change, of the American Mineralogist (MSA)
Cite as Authors (Year) Title. American Mineralogist, in press.
(DOI will not work until issue is live.) DOI: http://dx.doi.org/10.2138/am.2013.4364 7/11

nm for FA81, and from ~8 to~16 nm for FA100), the average particle sizes are similar to the calculated sizes (i.e., 27, 19, and 15 nm for FA51, FA81, and FA100, respectively). The particle size of γ, δ, and θ phases seems invariant upon annealing and drastically increases up to ~100 nm with phase transition into α-Al_2O_3 above 1473 K. This result is consistent with the result from previous electron microscopic observation [e.g., TEM and scanning electron microscope (SEM) images] (Nordahl and Messing, 2002; Wu et al., 1996).

Figure 3 presents the XRD patterns of as-received alumina nanoparticles and γ-Al_2O_3. The results show that the multiple phases of alumina exist in the samples: the XRD pattern for 27 nm alumina nanoparticles shows diffraction peaks for crystalline γ-, δ-, and θ-Al_2O_3, and those for 15 and 19 nm alumina nanoparticles mainly consists of γ- and δ-Al_2O_3. We note that the quantitative estimation of the fractions of alumina polymorphs in the nanoparticles using XRD is often difficult because metastable alumina phases are not well distinguished (Cava et al., 2007; Macedo et al., 2007). Furthermore, the diffraction peak positions (i.e., 2θ values) for metastable aluminas are similar (for instance, see diffraction peaks for δ- and θ-Al_2O_3 in Figure 3). Thus, we attempt to yield quantitative fraction of each alumina phase using NMR (see results and discussion below).

3.2. ^{27}Al MAS NMR Spectra

Figure 4A shows the ^{27}Al MAS NMR spectra at 11.7 T for 27, 19, and 15 nm alumina nanoparticles. The $^{[4]}$Al and $^{[6]}$Al peaks are well resolved at 0~20 and 50~80 ppm, respectively, showing unique quadrupolar peak shapes. The ^{27}Al MAS NMR spectrum for 27 nm alumina nanoparticles differs from those for 15 and 19 nm alumina nanoparticles and shows an additional sharp feature at ~10 ppm that is due to $^{[6]}$Al peak for θ-Al_2O_3 (in addition to γ- and δ-Al_2O_3) in the 27 nm alumina nanoparticles, as also indicated by the XRD result.

Figure 4B shows the ^{27}Al MAS NMR spectra for 27 nm alumina nanoparticles collected

This is a preprint, the final version is subject to change, of the American Mineralogist (MSA)
Cite as Authors (Year) Title. American Mineralogist, in press.
(DOI will not work until issue is live.) DOI: http://dx.doi.org/10.2138/am.2013.4364

at 9.4, 11.7, and 14.1 T. As the magnetic field (B_0) increases, the widths of the $^{[4]}$Al and $^{[6]}$Al peaks decrease because the contribution of quadrupolar broadening in the peak decreases with static magnetic field (i.e., quadrupolar broadening $\propto 1/B_0$) (Ashbrook and Duer, 2006; Duer, 2004; MacKenzie and Smith, 2002). Crystallographically distinct aluminum sites in γ-, δ-, and θ-Al_2O_3 are not fully resolved in the ^{27}Al MAS NMR spectra even at 11.7 T, mainly due to their similar peak positions for $^{[4,6]}$Al sites and disordered structure of γ- and δ-Al_2O_3. In the current ^{27}Al MAS NMR results, γ- and δ- Al_2O_3 are not well distinguished from each other. The lack of resolution between γ- and δ-Al_2O_3 in alumina nanoparticles is due to their similar atomic environments and pronounced topological disorder and thus to similarities in the peak positions of γ-, δ-, and θ-Al_2O_3 (Pecharroman et al., 1999): the δ-Al_2O_3 consists of a superlattice of the γ-Al_2O_3 structure with ordered cation vacancies (Jayaram and Levi, 1989). Simulation of the central transition peaks in these ^{27}Al MAS NMR spectra collected at varying static magnetic field allows us to quantitatively discriminate crystallographically distinct Al sites in metastable alumina nanoparticles (see section 3.3. below for further information).

Figure 5A–C present the ^{27}Al MAS NMR spectra at 11.7 T for 27, 19, and 15 nm alumina nanoparticles, respectively, with increasing annealing temperature up to 1573 K. The spectra show subtle, gradual changes in the quadrupolar peak shapes for the $^{[4]}$Al and $^{[6]}$Al sites. With increasing temperature up to 1473 K, an increase in the intensity of the sharp feature at ~10 ppm, the $^{[6]}$Al site in θ-Al_2O_3, is obvious. Though slight, changes in $^{[4]}$Al peak shape are indeed observed with increasing temperature, which may indicate changes in the atomic environment around Al during the phase transition γ → δ → θ-Al_2O_3 (see Figure 5D). Above 1473 K, a new $^{[6]}$Al peak for α-Al_2O_3 appears at ~14 ppm. The peak is partially resolved from the $^{[6]}$Al peaks for metastable aluminas owing to its symmetric shape and distinct peak position. The peak intensity for $^{[6]}$Al in α-Al_2O_3 increases dramatically with increasing temperature from 1473 K up to 1573 K: the peak intensity for $^{[4]}$Al decreases with increasing

This is a preprint, the final version is subject to change, of the American Mineralogist (MSA)
Cite as Authors (Year) Title. American Mineralogist, in press.
(DOI will not work until issue is live.) DOI: http://dx.doi.org/10.2138/am.2013.4364 7/11

temperature above 1473 K because the structure of α-Al_2O_3 has only a $^{[6]}$Al site.

Figure 5D compares the $^{[6]}$Al peaks in the ^{27}Al MAS NMR spectra of alumina nanoparticles with varying particle size at various temperatures. The fraction of α-Al_2O_3 in alumina nanoparticles annealed between 1473 K and 1573 K varies with the particle size. For instance, the phase transition into α-Al_2O_3 is apparently complete at 1523 K for 15 nm nanoparticles, with α-Al_2O_3 being the only Al site in the nanoparticles. Thus, the 15 nm alumina nanoparticles consist only of α-Al_2O_3 after annealing at 1523 K. However, the 19 and 27 nm nanoparticles still have a significant fraction of metastable aluminas at 1523 K. The phase transition into α-Al_2O_3 is apparently complete at ~1573 K for 27 and 19 nm alumina nanoparticles. These results indicate that transition temperature for θ → α-Al_2O_3 decreases with decreasing particle size.

3.3. Quantification of Metastable Alumina Phases in Nanoparticles

The quantitative fraction of each alumina polymorph in nanoparticles can be estimated from the analysis of the unique quadrupolar peak shape for each Al sites with NMR parameters including C_q, η, and δ_{iso}. The NMR parameters for $^{[4,6]}$Al sites in the metastable aluminas studied in previous and current studies are given in Table 1. Although the NMR parameters for the $^{[4,6]}$Al sites of θ- and α-Al_2O_3 were generally confirmed, those for γ-Al_2O_3 show a wide range of variation (Hagaman et al., 2010; Kraus et al., 1996; O'Dell et al., 2007; Pecharroman et al., 1999; Sabarinathan et al., 2010; Skibsted et al., 1991): reported C_q values for the $^{[6]}$Al site in γ-Al_2O_3 varies from 4±1 to 7.5±1 MHz (Hagaman et al., 2010; Kraus et al., 1996; Perander et al., 2007). Additionally, the NMR parameters for the $^{[4,6]}$Al sites in δ-Al_2O_3 have not been reported. The simultaneous simulation of ^{27}Al NMR spectra collected at different magnetic fields allows us to obtain robust NMR parameters (O'Dell et al., 2007; Perander et al., 2007). In the current study, following protocols has been used to obtain NMR parameters for

This is a preprint, the final version is subject to change, of the American Mineralogist (MSA)
Cite as Authors (Year) Title. American Mineralogist, in press.
(DOI will not work until issue is live.) DOI: http://dx.doi.org/10.2138/am.2013.4364 7/11

the Al sites in the alumina phases. First, we roughly simulated the spectra at 11.7 T using the previously reported NMR parameters for each phase (Table 1). Then, we adjusted the detailed NMR parameters by simulating the spectra collected at 9.4 T, 11.7, and 14.1 T simultaneously, with a constraints of intensity ratio between $^{[4]}$Al and $^{[6]}$Al for each alumina phase. Detailed information on the NMR parameters for alumina nanoparticles studied in the current study is also given in Table 2.

Figure 6 shows the ^{27}Al MAS NMR spectra that were simulated simultaneously at 9.4, 11.7, and 14.1 T. The simulation of the $^{[4]}$Al and $^{[6]}$Al peaks for (γ, δ)-Al_2O_3 in the ^{27}Al MAS NMR spectrum were performed using the Czjzek model (de Lacaillerie et al., 2008; Lee et al., 2009a; Massiot et al., 2002; Neuville et al., 2004). Taking into consideration expected similarity between NMR parameters for $^{[4,6]}$Al sites in (γ, δ)-Al_2O_3, we consider a single $^{[4]}$Al and $^{[6]}$Al peak for (γ, δ)-Al_2O_3. The average C_q and δ_{iso} for $^{[4]}$Al in (γ, δ)-Al_2O_3 are 5.7±1.0 MHz and 72±3 ppm, respectively, and those for $^{[6]}$Al are 4.2±1.0 MHz and 14±3 ppm. We also collected the ^{27}Al MAS NMR spectrum for standard γ-Al_2O_3 [single phase, Sigma Aldrich, product no. 544833, mixture of nanorods (~ 50 nm length) and nanoparticles (~ 10 nm diameter)]. The spectrum was also simulated well with similar approach: δ_{iso} = 72.5±3.0 ppm, C_q = 5.7±1.0 MHz for the $^{[4]}$Al site and δ_{iso} = 14±2 ppm, C_q = 4.7±1.0 MHz for the $^{[6]}$Al site. These NMR parameters for the $^{[4,6]}$Al sites in (γ, δ)-Al_2O_3 show intermediate value between those reported in previous studies of γ-Al_2O_3 (Hagaman et al., 2010; Kraus et al., 1996; O'Dell et al., 2007; Pecharroman et al., 1999; Perander et al., 2007).

We note that there is a minor but detectable difference in NMR line shape for $^{[6]}$Al sites and relative peak intensity ($^{[4]}$Al/$^{[6]}$Al) in the standard γ-phase (from Sigma Aldrich, 544833) and the γ-Al_2O_3 in the mixed phases, indicating that the particle size and morphology of the particles may lead to a slight change in structural distortion and thus NMR parameters. Similar particle size effect on NMR parameters, particularly C_q, has been observed for α-

This is a preprint, the final version is subject to change, of the American Mineralogist (MSA)
Cite as Authors (Year) Title. American Mineralogist, in press.
(DOI will not work until issue is live.) DOI: http://dx.doi.org/10.2138/am.2013.4364

303 alumina nanoparticles (Sabarinathan et al., 2010). Currently, the changes in these NMR
304 parameters are relatively small (see Table 2) and thus are within uncertainty. Yet this
305 potentially interesting effect of particle size remains to be explored.

306 The ^{27}Al NMR parameters for θ-Al_2O_3 are δ_{iso} = 80.5 ppm, C_q = 6.0 MHz, and η_q = 0.7 for
307 the $^{[4]}$Al site and δ_{iso} = 10.5 ppm, C_q = 3.45 MHz, and η = 0.0 for the $^{[6]}$Al site, respectively.
308 These results are consistent with those from previous studies (O'Dell et al., 2007; Pecharroman
309 et al., 1999). Note that the quadrupolar NMR parameters are correlated with deviation from
310 perfect tetrahedral or octahedral symmetry (Ghose and Tsang, 1973). The current results
311 imply that deviation from perfect cubic symmetry for Al site in θ-Al_2O_3 is larger than those for
312 γ-Al_2O_3. In contrast, as also deduced from XRD patterns, the dispersion of NMR parameters
313 for Al sites in γ- and δ-Al_2O_3 phases indicate a moderate degree of structural disorder around
314 Al sites in γ- and δ-Al_2O_3 as previously reported (Lippens and Deboer, 1964). θ-Al_2O_3 shows
315 less disordered structures as indicated by narrow dispersions in the NMR spectra and XRD
316 patterns (Figures 3 and 5).

317 Figure 7 shows the simulated ^{27}Al MAS NMR spectra for alumina nanoparticles with
318 varying particle size and annealing temperature, which provides the quantitative changes in
319 the fractions of each alumina phase in the nanoparticles (see supporting on-line materials for
320 the complete sets of NMR spectra with varying temperature). For the NMR parameters of the
321 $^{[6]}$Al site in α-Al_2O_3, we follow the previously reported values (i.e., δ_{iso} = 15.9 ppm, C_q = 2.4
322 MHz, and η_q = 0) (Kraus et al., 1998; O'Dell et al., 2007; Sabarinathan et al., 2010; Skibsted et al.,
323 1991). The intensity ratio between the $^{[4]}$Al and $^{[6]}$Al sites in θ-Al_2O_3 is ~50±5:50±5, which is
324 consistent with the previously reported ratio for the ideal structure of θ-Al_2O_3 (O'Dell et al.,
325 2007; Pecharroman et al., 1999). Though indirect, $^{[4]}$Al and $^{[6]}$Al ratio in the (γ, δ)-Al_2O_3 may
326 provide quantitative fraction of γ- and δ-Al_2O_3. The ratios between $^{[4]}$Al and $^{[6]}$Al for (γ, δ)-
327 Al_2O_3 in 15, 19, and 27 nm alumina nanoparticles are ~26±8:74±8, 30±8:70±8, and 32±8:68±8,

This is a preprint, the final version is subject to change, of the American Mineralogist (MSA)
Cite as Authors (Year) Title. American Mineralogist, in press.
(DOI will not work until issue is live.) DOI: http://dx.doi.org/10.2138/am.2013.4364

328 respectively. These are intermediate between the values for the ideal structures of γ- and δ-
329 Al_2O_3: the $^{[4]}$Al:$^{[6]}$Al ratios in ideal γ- and δ-Al_2O_3 are about 25:75 and 38:62, respectively
330 (Pecharroman et al., 1999; Repelin and Husson, 1990). The current result may indicate that the
331 fraction of γ-Al_2O_3 is more significant in a smaller nanoparticles, because the $^{[4]}$Al:$^{[6]}$Al ratio in
332 (γ, δ)-Al_2O_3 approaches the ideal ratio for γ-Al_2O_3 as the particle size decreases from 27 nm to
333 15 nm. The fraction of each alumina phase in alumina nanoparticles based on NMR results in
334 the current remains to be tested with other quantitative experimental techniques.

335 Figure 8A–C show the variations in the population of each alumina phase in 27, 19,
336 and 15 nm alumina nanoparticles, respectively, with increasing annealing temperature up to
337 1573 K, which demonstrates the effect of particle size on the stability field for alumina
338 polymorphs. The population of alumina polymorphs in as-received alumina nanoparticles
339 varies with the particle size. The (γ, δ)-Al_2O_3: θ-Al_2O_3 ratio is approximately 99±0.5:1±0.5,
340 96±2:4±2, and 80±3:20±3 for the 15, 19, and 27 nm alumina nanoparticles, respectively. With
341 increasing temperature above ~873 K, the population of θ-Al_2O_3 gradually increases up to
342 ~1473 K at the expense of (γ, δ)-Al_2O_3. The fractions of θ-Al_2O_3 after annealing at 1473 K are
343 ~16±5%, 18±5%, and 38±5% for 15, 19, and 27 nm alumina nanoparticles, respectively, and
344 thus a major fraction (62%~84%) of the alumina nanoparticles exist as (γ, δ)-Al_2O_3. The error
345 bar in the fraction of each alumina phase stems from the deviation from a perfect match
346 between experimental and simulated spectra (~3%), the contribution from the uncertainties in
347 estimated NMR parameters (~3%), and possible artifacts introducing fixed value for NMR
348 parameters upon simulations (~3%). Taking into consideration of those uncertainties, the total
349 error bar of ±5 % is estimated. The significant fraction of (γ, δ)-Al_2O_3 in the nanoparticles at
350 1473 K is somewhat unexpected, considering the previously known transition temperatures
351 for γ → δ-Al_2O (700–800°C) and δ → θ-Al_2O (900–1000°C) (Levin and Brandon, 1998 and
352 references therein). However, the presence of γ-Al_2O_3 above 1473 K also has been reported in

This is a preprint, the final version is subject to change, of the American Mineralogist (MSA)
Cite as Authors (Year) Title. American Mineralogist, in press.
(DOI will not work until issue is live.) DOI: http://dx.doi.org/10.2138/am.2013.4364

previously XRD studies for both nanocrystalline and bulk alumina (heating rate of 3-50 K/min) (Bokhimi et al., 2001; Gan et al., 2009). Note that kinetic broadening upon phase transition among nanoparticles may contribute to the presence of larger fractions of (γ, δ)-Al_2O_3. This effect of kinetic broadening on phase transition needs to be explored using further NMR studies with varying annealing time.

Figure 8D–F (enlarged plots of Figure 8A–C) shows the variation in the population of alumina phases between ~1400 and ~1600 K for alumina nanoparticles. Multiple phases of alumina including γ-, δ-, θ-, and α-Al_2O_3 coexist in alumina nanoparticles from ~1473 K to the temperature at which all phase transitions into α-Al_2O_3 are complete (i.e., ~1573 K for 27 and 19 nm nanoparticles and ~1523 K for 15 nm nanoparticles). With increasing temperature from ~1473 K to ~1573 K, the population of α-Al_2O_3 increases dramatically at the expense of the metastable aluminas. The transition temperature for γ, δ, θ → α-Al_2O_3 decreases with decreasing particle size. In this study, the transition temperature for γ, δ, θ → α-Al_2O_3 is defined by the temperature of which the 50 % of alumina nanoparticles exist in form of α-Al_2O_3. Although the phase transition γ, δ → θ-Al_2O_3 occurs gradually with increasing annealing temperature from 873 K to 1473 K, the phase transitions γ, δ → α-Al_2O_3 and θ → α-Al_2O_3 occur dramatically within a narrow temperature range between 1473 K and 1573 K.

3.4. ^{27}Al 3QMAS NMR Spectra

Figure 9A and 9B show the ^{27}Al 3QMAS NMR spectra for 27 nm alumina nanoparticles before and after annealing at 1497 K for 2 h; the resolution is considerably better than that of the ^{27}Al MAS NMR spectra. The crystallographically distinct $^{[6]}$Al and $^{[4]}$Al sites in (γ, δ)- and θ-Al_2O_3 as well as α-Al_2O_3 are resolved in the isotropic dimension. For robust peak assignment, we calculated the expected position for the center of gravity of the $^{[4,6]}$Al sites in γ-, θ-, and α-Al_2O_3 using previously reported NMR parameters shown in Table 1. Figure 9C shows the

expected position of the center of gravity of the $^{[4,6]}$Al sites for γ-, θ-, and α-Al_2O_3 in ^{27}Al 3QMAS NMR spectra (Hagaman et al., 2010; Kraus et al., 1996; O'Dell et al., 2007; Pecharroman et al., 1999; Perander et al., 2007; Sabarinathan et al., 2010; Skibsted et al., 1991). On the basis of plots in figure 9C, the peak at -10 ppm in the isotropic dimension is assigned to the $^{[6]}$Al site in α-Al_2O_3, which appears after annealing at 1497 K (Hagaman et al., 2010; Kraus et al., 1996; O'Dell et al., 2007; Sabarinathan et al., 2010; Skibsted et al., 1991). The peaks at -8 ppm and -53 ppm in the isotropic dimension are assigned to the $^{[6]}$Al and $^{[4]}$Al sites in θ-Al_2O_3, respectively (O'Dell et al., 2007; Pecharroman et al., 1999). These $^{[6]}$Al and $^{[4]}$Al peak intensities for θ-Al_2O_3 increase after annealing at 1497 K, following the γ, δ → θ phase transition. The broad peaks ranging from -10 to -20 ppm and at ~ -45 ppm are assigned to unresolved $^{[6]}$Al and $^{[4]}$Al sites in γ- and δ-Al_2O_3, respectively as their intensities decrease significantly after annealing at 1497 K (Hagaman et al., 2010; Kraus et al., 1996; Perander et al., 2007). These results are consistent with the temperature-induced phase transition sequence of alumina (i.e., γ → δ → θ → α-Al_2O_3).

Figure 10 shows the ^{27}Al 3QMAS NMR spectra for alumina nanoparticles with varying particle size and annealing temperature; the $^{[4]}$Al and $^{[6]}$Al peaks for (γ, δ)-, θ-, and α-Al_2O_3 are resolved (see supporting on-line materials for the complete sets of NMR spectra with varying temperature). The $^{[4,6]}$Al peaks for θ-Al_2O_3 are observed in the ^{27}Al 3QMAS NMR spectra for the 15 and 19 nm alumina nanoparticles as well as the 27 nm alumina nanoparticles. We note that the presence of θ-Al_2O_3 is not clear in the XRD patterns for 15 nm and 19 nm alumina nanoparticles (see Figure 3). The discrepancy may be due to that small fraction (~3±2 %) of θ-Al_2O_3 is not detected using XRD. As the annealing temperature increases to ~1473 K, the peak intensities for the $^{[4,6]}$Al sites in (γ, δ)-Al_2O_3 decrease, whereas those for θ-Al_2O_3 increase. Above 1473 K, the $^{[6]}$Al peak for α-Al_2O_3 is observed, indicating the onset of the θ → α phase transition. These results are consistent with those of the ^{27}Al MAS NMR spectra.

This is a preprint, the final version is subject to change, of the American Mineralogist (MSA)
Cite as Authors (Year) Title. American Mineralogist, in press.
(DOI will not work until issue is live.) DOI: http://dx.doi.org/10.2138/am.2013.4364 7/11

403

404 **3.5. Effect of Particle Size on Phase Transitions of Metastable Alumina**

405 Several phase transitions in alumina nanoparticles observed in the current study
406 include, (1) γ, δ → θ-Al_2O_3, (2) γ, δ → α-Al_2O_3, and (3) θ → α-Al_2O_3. Although the phase
407 transition γ, δ → θ-Al_2O_3 occurs gradually within a broad temperature range between ~ 873 K
408 and 1473 K, both phase transitions, γ, δ → α-Al_2O_3 and θ → α-Al_2O_3 occurs within narrow
409 temperature range between ~ 1473 K and 1573 K. The different temperature range between
410 phase transition γ, δ → θ and γ, δ, θ → α may originate from the different structural disorder
411 between the metastable aluminas (i.e., γ-, δ-, θ-) and α-Al_2O_3. The configurational disorder of γ-
412 and δ-Al_2O_3 may induce a gradual γ, δ → θ phase transition from 873 K to 1473 K as has been
413 observed for structural transitions in compressed amorphous oxides (see (Lee et al., 2008).

414 Figure 11 presents the normalized variation in the (γ, δ)-, θ- and α-Al_2O_3 population
415 with varying particle size and annealing temperature. The normalized variations of (γ, δ)- and
416 θ-Al_2O_3 population in 27, 19, and 15 nm nanoparticles between 298 K and ~1473 K are similar
417 to each other, indicating that the effect of particle size on the phase transition (γ, δ) → θ-Al_2O_3
418 is not significant. On the other hand, effect of particle size on the variation of α-Al_2O_3
419 population is obvious between ~ 1473 K and ~ 1673 K. The transition temperature for γ, δ, θ →
420 α-Al_2O_3, where a 50 % for alumina is α-Al_2O_3, is 1523±10, 1518±10, and 1490±10 K for 27, 19,
421 and 15 nm alumina nanoparticles, respectively. This result indicates that the phase transition γ,
422 δ, θ → α-Al_2O_3 occurs at lower temperatures for smaller alumina nanoparticles. Although the
423 transition temperature in this study may change with the annealing time because the
424 equilibrium or steady state for phase transitions of alumina may not be reached with an
425 annealing duration of 2 h, the current results can yield insights into the relative difficulty for
426 phase transition γ, δ, θ → α-Al_2O_3. This could be due to higher surface energy of θ-Al_2O_3 than
427 that of α-Al_2O_3 and/or it could be due to the fact that transition from θ-Al_2O_3 to α-Al_2O_3 is

This is a preprint, the final version is subject to change, of the American Mineralogist (MSA)
Cite as Authors (Year) Title. American Mineralogist, in press.
(DOI will not work until issue is live.) DOI: http://dx.doi.org/10.2138/am.2013.4364

428 kinetically favored for smaller nanoparticles. A detailed study for surface energy of θ-Al_2O_3
429 phase remains to be explored.

430 In this study, we quantified the fractions of alumina polymorphs in nanoparticles and
431 reported the NMR characteristics of their Al sites using both high-resolution 1D ^{27}Al MAS and
432 3QMAS NMR. Particularly, first 2D NMR spectra for complex nanoparticles resolved
433 crystallographically distinct $^{[6]}$Al and $^{[4]}$Al sites in (γ, δ)- and θ-Al_2O_3. The results show that
434 phase transition γ, δ → θ-Al_2O_3 occurs gradually with increasing annealing temperature from
435 873 K to 1473 K and the phase transitions γ, δ, θ → α-Al_2O_3 occur dramatically within a narrow
436 temperature range between 1473 K and 1573 K. In addition to that, the results clearly
437 demonstrate that phase transition γ, δ, θ → α-Al_2O_3 occurs at lower temperatures for smaller
438 alumina nanoparticles. The current results may be helpful to account for a transition behavior
439 in other simple and complex oxide nanoparticles. Nanoparticles with complex compositions
440 are produced through geochemical (Banfield and Zhang, 2001; Foissner et al., 2009; Hochella
441 et al., 2008) and mechanical processes (Han et al., 2007) in diverse geological settings.
442 Although the alumina nanoparticles in this study are not ubiquitous in the earth, they are the
443 simplest compound that exhibits the complexities of diverse earth materials. In addition to
444 Al_2O_3, other minerals including Fe_2O_3, TiO_2, and ZrO_2 also exhibit different surface energies
445 among stable and metastable polymorphs, indicating a similar effect of particle size on their
446 relative stability in nanoparticles (Navrotsky, 2004). The potential metastability of earth
447 materials in nano-sized domain may induce heterogeneity of mantle (e.g., nanoscale spinel
448 phases at the olivine-spinel transition at 400 km depth) (Banfield and Zhang, 2001). The
449 structural information on alumina polymorphs and the mechanistic details obtained from the
450 experiments described here provide insights into the nature of the phase transitions of other
451 oxide nanoparticles, highlighting the effects of particle size.

452

Acknowledgment

This research was supported by Korean Science and Engineering Foundation grants through the National Research Laboratory Program (2012-026-411) and partly supported by the Korea Meteorological Administration Research and Development Program under Grant CATER 2012-8030. We deeply appreciate constructive and careful suggestions by the two anonymous reviewers, Dr. Ganapathy, and Dr. Phillips.

References

Ashbrook, S.E., and Duer, M.J. (2006) Structural information from quadrupolar nuclei in solid state NMR. Concepts Magn. Reson. Part A, 28A(3), 183-248.

Ashbrook, S.E., and Smith, M.E. (2006) Solid state O-17 NMR - an introduction to the background principles and applications to inorganic materials. Chem. Soc. Rev., 35(8), 718-735.

Banfield, J.F., and Zhang, H.Z. (2001) Nanoparticles in the environment. Nanoparticles and the Environment, 44, p. 1-58. Mineralogical Soc America, Washington.

Blonski, S., and Garofalini, S.H. (1993) Molecular-dynamics simulations of α-alumin and γ-alumina surfaces. Surf. Sci., 295(1-2), 263-274.

Bokhimi, X., Toledo-Antonio, J.A., Guzman-Castillo, M.L., Mar-Mar, B., Hernandez-Beltran, F., and Navarrete, J. (2001) Dependence of boehmite thermal evolution on its atom bond lengths and crystallite size. J. Solid State Chem., 161(2), 319-326.

Chupas, P.J., Ciraolo, M.F., Hanson, J.C., and Grey, C.P. (2001) In situ X-ray diffraction and solid-state NMR study of the fluorination of γ-Al_2O_3 with HCF_2Cl. J. Am. Chem. Soc., 123(8), 1694-1702.

Damodaran, K., Rajamohanan, P.R., Chakrabarty, D., Racherla, U.S., Manohar, V., Fernandez, C., Amoureux, J.P., and Ganapathy, S. (2002) Triple-quantum magic angle spinning ^{27}Al NMR of aluminum hydroxides. J. Am. Chem. Soc., 124(13), 3200-3201.

de Lacaillerie, J.B.D., Fretigny, C., and Massiot, D. (2008) MAS NMR spectra of quadrupolar nuclei in disordered solids: The Czjzek model. J. Magn. Reson., 192(2), 244-251.

Duer, M.J. (2004) Introduction to solid-state NMR spectroscopy. Blackwell

Fitzgerald, J.J., Piedra, G., Dec, S.F., Seger, M., and Maciel, G.E. (1997) Dehydration studies of a high-surface-area alumina (pseudo-boehmite) using solid-state ^{1}H and ^{27}Al NMR. J. Am. Chem. Soc., 119(33), 7832-7842.

Foissner, W., Weissenbacher, B., Krautgartner, W.D., and Lutz-Meindl, U. (2009) A cover of glass: First report of biomineralized silicon in a ciliate, Maryna umbrellata (ciliophora:

Colpodea). J. Eukaryot. Microbiol., 56(6), 519-530.

Gan, B.K., Madsen, I.C., and Hockridge, J.G. (2009) In situ X-ray diffraction of the transformation of gibbsite to alpha-alumina through calcination: effect of particle size and heating rate. J. Appl. Crystallogr., 42, 697-705.

Hagaman, E.W., Jiao, J.A., Chen, B.H., Ma, Z., Yin, H.F., and Dai, S. (2010) Surface alumina species on modified titanium dioxide: A solid-state ^{27}Al MAS and 3QMAS NMR investigation of catalyst supports. Solid State Nucl. Magn. Reson., 37(3-4), 82-90.

Han, R., Shimamoto, T., Hirose, T., Ree, J.H., and Ando, J. (2007) Ultralow friction of carbonate faults caused by thermal decomposition. Science, 316(5826), 878-881.

Hochella, M.F., Jr., Lower, S.K., Maurice, P.A., Penn, R.L., Sahai, N., Sparks, D.L., and Twining, B.S. (2008) Nanominerals, Mineral Nanoparticles, and Earth Systems. Science, 319(5870), 1631-1635.

Jayaram, V., and Levi, C.G. (1989) The structure of δ-alumina evolved from the melt and the γ–δ transformation. Acta Metall., 37(2), 569-578.

John, C.S., Alma, N.C.M., and Hays, G.R. (1983) Characterization of transitional alumina by solid-state magic angle spinning aluminum NMR. Appl. Catal., 6(3), 341-346.

Kentgens, A.P.M., and Verhagen, R. (1999) Advantages of double frequency sweeps in static, MAS and MQMAS NMR of spin I=3/2 nuclei. Chem. Phys. Lett., 300(3-4), 435-443.

Kraus, H., Muller, M., Prins, R., and Kentgens, A.P.M. (1998) Comments on the ^{27}Al NMR visibility of aluminas. J. Phys. Chem. B, 102(20), 3862-3865.

Kraus, H., Prins, R., and Kentgens, A.P.M. (1996) A ^{27}Al MQMAS and off-resonance nutation NMR investigation of Mo-P/gamma-Al_2O_3 hydrotreating catalyst precursors. J. Phys. Chem., 100(40), 16336-16345.

Kresse, G., Schmid, M., Napetschnig, E., Shishkin, M., Kohler, L., and Varga, P. (2005) Structure of the ultrathin aluminum oxide film on NiAl(110). Science, 308(5727), 1440-1442.

Kryukova, G.N., Klenov, D.O., Ivanova, A.S., and Tsybulya, S.V. (2000) Vacancy ordering in

513 the structure of γ-Al_2O_3. J. Eur. Ceram. Soc. , 20(8), 1187-1189.

514 Lee, S.K. (2005) Microscopic origins of macroscopic properties of silicate melts and glasses at
515 ambient and high pressure: Implications for melt generation and dynamics. Geochim.
516 Cosmochim. Ac. , 69(14), 3695-3710.

517 Lee, S.K., Deschamps, M., Hiet, J., Massiot, D., and Park, S.Y. (2009a) Connectivity and
518 proximity between quadrupolar nuclides in oxide glasses: Insights from through-bond
519 and through-space correlations in solid-state NMR. J. Phys. Chem. B, 113(15), 5162-5167.

520 Lee, S.K., Eng, P.J., Mao, H.K., and Shu, J.F. (2008) Probing and modeling of pressure-induced
521 coordination transformation in borate glasses: Inelastic x-ray scattering study at high
522 pressure. Phys. Rev. B, 78(21).

523 Lee, S.K., Kim, H.N., Lee, B.H., Kim, H.I., and Kim, E.J. (2010a) Nature of chemical and
524 topological disorder in borogermanate glasses: Insights from B-11 and O-17 solid-State
525 NMR and quantum chemical calculations. J. Phys. Chem. B 114(1), 412-420.

526 Lee, S.K., Lee, S.B., Park, S.Y., Yi, Y.S., and Ahn, C.W. (2009b) Structure of amorphous
527 aluminum oxide. Phys. Rev. Lett., 103(9), 095501.

528 Lee, S.K., Park, S.Y., Yi, Y.S., and Moon, J. (2010b) Structure and disorder in amorphous
529 alumina thin films: Insights from high-resolution solid-state NMR. J. Phys. Chem. C
530 114(32), 13890-13894.

531 Lee, S.K., and Stebbins, J.F. (2003) O atom sites in natural kaolinite and muscovite: ^{17}O MAS
532 and 3QMAS NMR study. Am. Mineral., 88(4), 493-500.

533 Lee, S.K., Stebbins, J.F., Weiss, C.A., and Kirkpatrick, R.J. (2003) O-17 and Al-27 MAS and
534 3QMAS NMR study of synthetic and natural layer silicates. Chem. Mater., 15(13), 2605-
535 2613.

536 Lee, S.K., and Weiss, C.A. (2008) Multiple oxygen sites in synthetic phyllosilicates with
537 expandable layers: ^{17}O solid-state NMR study. Am. Mineral., 93(7), 1066-1071.

538 Levin, I., Bendersky, L.A., Brandon, D.G., and Ruhle, M. (1997) Cubic to monoclinic phase
539 transformations in alumina. Acta Materialia, 45(9), 3659-3669.

Levin, I., and Brandon, D. (1998) Metastable alumina polymorphs: Crystal structures and transition sequences. J. Am. Ceram. Soc., 81(8), 1995-2012.

Lin, J.F., Degtyareva, O., Prewitt, C.T., Dera, P., Sata, N., Gregoryanz, E., Mao, H.K., and Hemley, R.J. (2004) Crystal structure of a high-pressure/high-temperature phase of alumina by in situ X-ray diffraction. Nat. Mater. , 3(6), 389-393.

Liu, S.F., Zhang, L.G., and An, L.N. (2005) Phase transformation of mechanically milled nano-sized γ-alumina. J. Am. Ceram. Soc., 88(9), 2559-2563.

Macedo, M.I.F., Bertran, C.A., and Osawa, C.C. (2007) Kinetics of the γ → α-alumina phase transformation by quantitative X-ray diffraction. J. Mater. Sci., 42(8), 2830-2836.

MacKenzie, K.J.D., and Smith, M.E. (2002) Multinuclear Solid-State NMR of Inorganic Materials. Pergamon.

Madhu, P.K., Goldbourt, A., Frydman, L., and Vega, S. (1999) Sensitivity enhancement of the MQMAS NMR experiment by fast amplitude modulation of the pulses. Chem. Phys. Lett., 307(1-2), 41-47.

Massiot, D., Conanec, R., Feldmann, W., Marchand, R., and Laurent, Y. (1996) NMR characterization of the $Na_3AlP_3O_9N$ and $Na_2Mg_2P_3O_9N$ nitridophosphates: Location of the $(NaAl)/Mg^{-2}$ substitution. Inorg. Chem., 35(17), 4957-4960.

Massiot, D., Fayon, F., Capron, M., King, I., Le Calve, S., Alonso, B., Durand, J.O., Bujoli, B., Gan, Z.H., and Hoatson, G. (2002) Modelling one- and two-dimensional solid-state NMR spectra. Magn. Reson. Chem., 40(1), 70-76.

Mastikhin, V.M., Krivoruchko, O.P., Zolotovskii, B.P., and Buyanov, R.A. (1981) Study of local environment and cation distribution in Al-(III) oxides by ^{27}Al NMR with sample rotation at a magic angle. React. Kinet. Catal. Lett., 18(1-2), 117-120.

McHale, J.M., Auroux, A., Perrotta, A.J., and Navrotsky, A. (1997a) Surface energies and thermodynamic phase stability in nanocrystalline aluminas. Science, 277(5327), 788-791.

McHale, J.M., Navrotsky, A., and Perrotta, A.J. (1997b) Effects of increased surface area and

566 chemisorbed H_2O on the relative stability of nanocrystalline gamma-Al_2O_3 and alpha-
567 Al_2O_3. J. Phys. Chem. B 101(4), 603-613.

568 Navrotsky, A. (2001) Thermochemistry of nanomaterials. In J.F. Banfield, and A. Navrotsky,
569 Eds. Nanoparticles and the Environment, 44, p. 73-103.

570 -. (2004) Energetic clues to pathways to biomineralization: Precursors, clusters, and
571 nanoparticles. Proc. Natl. Acad. Sci. U. S. A., 101(33), 12096-12101.

572 Neuville, D.R., Cormier, L., and Massiot, D. (2004) Al environment in tectosilicate and
573 peraluminous glasses: A Al-27 MQ-MAS NMR, Raman, and XANES investigation.
574 Geochim. Cosmochim. Ac., 68(24), 5071-5079.

575 Nordahl, C.S., and Messing, G.L. (2002) Sintering of α-Al_2O_3-seeded nanocrystalline γ-Al_2O_3
576 powders. J. Eur. Ceram. Soc., 22(4), 415-422.

577 O'Dell, L.A., Savin, S.L.P., Chadwick, A.V., and Smith, M.E. (2007) A ^{27}Al MAS NMR study of
578 a sol-gel produced alumina: Identification of the NMR parameters of the θ-Al_2O_3
579 transition alumina phase. Solid State Nucl. Magn. Reson., 31(4), 169-173.

580 Ollivier, B., Retoux, R., Lacorre, P., Massiot, D., and Ferey, G. (1997) Crystal structure of
581 kappa-alumina: An X-ray powder diffraction, TEM and NMR study. J. Mater. Chem.,
582 7(6), 1049-1056.

583 Pecharroman, C., Sobrados, I., Iglesias, J.E., Gonzalez-Carreno, T., and Sanz, J. (1999) Thermal
584 evolution of transitional aluminas followed by NMR and IR spectroscopies. J. Phys.
585 Chem. B, 103(30), 6160-6170.

586 Perander, L.M., Zujovic, Z.D., Groutso, T., Hyland, M.M., Smith, M.E., O'Dell, L.A., and
587 Metson, J.B. (2007) Characterization of metallurgical-grade aluminas and their
588 precursors by ^{27}AI NMR and XRD. Can. J. Chem.-Rev. Can. Chim., 85(10), 889-897.

589 Phillips, B.L. (2000) NMR spectroscopy of phase transitions in minerals. Transformation
590 Processes in Minerals, 39, 203-240.

591 Piedra, G., Fitzgerald, J.J., Dando, N., Dec, S.F., and Maciel, G.E. (1996) Solid-state ^{1}H NMR
592 studies of aluminum oxide hydroxides and hydroxides. Inorg. Chem., 35(12), 3474-3478.

593 Pinto, H.P., Nieminen, R.M., and Elliott, S.D. (2004) Ab initio study of gamma-Al_2O_3 surfaces.
594 Phys. Rev. B 70(12).

595 Rajendran, S. (1994) Production of ultrafine α-alumina powders and fabrication of fine-
596 grained strong ceramics. J. Mater. Sci., 29(21), 5664-5672.

597 Repelin, Y., and Husson, E. (1990) Structureal studies on transition aluminas. 1. γ-alumina and
598 δ-alumina Mat. Res. Bull., 25(5), 611-621.

599 Sabarinathan, V., Ramasamy, S., and Ganapathy, S. (2010) Perturbations to ^{27}Al Electric Field
600 Gradients in Nanocrystalline α-Al_2O_3 Studied by High-Resolution Solid-State NMR. J.
601 Phys. Chem. B 114(5), 1775-1781.

602 Santos, H.D., and Santos, P.D. (1992) Pseudomorphic formation of aluminas from fibrillar
603 pseudoboehmite. Mater. Lett., 13(4-5), 175-179.

604 Skibsted, J., Nielsen, N.C., Bildsoe, H., and Jakobsen, H.J. (1991) Satellite transitions in MAS
605 NMR-spectra of quadrupolar nuclei. J. Magn. Reson., 95(1), 88-117.

606 Stebbins, J.F., Kroeker, S., Lee, S.K., and Kiczenski, T.J. (2000) Quantification of five- and six-
607 coordinated aluminum ions in aluminosilicate and fluoride-containing glasses by high-
608 field, high-resolution Al-27 NMR. J. Non-Cryst. Solids 275(1-2), 1-6.

609 Stebbins, J.F., Lee, S.K., and Oglesby, J.V. (1999) Al-O-Al oxygen sites in crystalline aluminates
610 and aluminosilicate glasses: High-resolution oxygen-17 NMR results. Am. Mineral.,
611 84(5-6), 983-986.

612 Tangeman, J.A., Phillips, B.L., Nordine, P.C., and Weber, J.K.R. (2004) Thermodynamics and
613 structure of single- and two-phase yttria-alumina glasses. J. Phys. Chem. B, 108(30),
614 10663-10671.

615 Wu, S.J., DeJonghe, L.C., and Rahaman, M.N. (1996) Sintering of nanophase γ-Al_2O_3 powder. J.
616 Am. Ceram. Soc., 79(8), 2207-2211.

617 Xue, X.Y., Kanzaki, M., and Fukui, H. (2010) Unique crystal chemistry of two polymorphs of
618 topaz-OH: A multi-nuclear NMR and Raman study. Am. Mineral., 95(8-9), 1276-1293.

619 Yang, X., Pierre, A.C., and Uhlmann, D.R. (1988) TEM study of boehmite gels and their

This is a preprint, the final version is subject to change, of the American Mineralogist (MSA)
Cite as Authors (Year) Title. American Mineralogist, in press.
(DOI will not work until issue is live.) DOI: http://dx.doi.org/10.2138/am.2013.4364

620 transformation to α-alumina. J. Non-Cryst. Solids 100(1-3), 371-377.

This is a preprint, the final version is subject to change, of the American Mineralogist (MSA)
Cite as Authors (Year) Title. American Mineralogist, in press.
(DOI will not work until issue is live.) DOI: http://dx.doi.org/10.2138/am.2013.4364

621 **Table 1.** ^{27}Al NMR parameters for metastable and α alumina

Phase	$^{[n]}$Al	Larmor frequency (MHz)	C_q (MHz)	η	δ_{iso} (ppm)	Reference
(γ, δ)	$^{[6]}$Al	130.3	4.5±1	-	14±3	This work
	$^{[4]}$Al	130.3	5.7±1	-	72±3	This work
γ	$^{[6]}$Al	130.3	4.6±1	-	14±3	This work
		93.81	7±1	-	16±2	Perander et al., 2007
		130.32	4.5±0.5	0.3	9±1	Kraus et al., 1996
		182.4	4±1	0.8±0.1	8±2	Hagaman et al., 2010
		182.4	7.5±1	0.8±0.1	10±2	Hagaman et al., 2010
	$^{[4]}$Al	130.3	5.7±1	-	72±3	This work
		93.81	5.5±3	-	71±2	Perander et al., 2007
		130.32	5±0.5	0.3	67±1	Kraus et al., 1996
		182.4	6±1	0.6±0.1	74±5	Hagaman et al., 2010
θ	$^{[6]}$Al	104.3	3.45±0.2	0±0.1	10.5±0.3	This work
		156.4	3.5±0.3	0+0.1	10.5±0.3	O'Dell et al., 2007
		104.23	3.1±0.2	0.4±0.1	11.3±0.7	Pecharroman et al., 1999
	$^{[4]}$Al	104.3	6.15±0.2	0.7±0.1	80.5±1.0	This work
		156.4	6.4±0.1	0.65±0.02	80±0.5	O'Dell et al., 2007
		104.23	5.5±0.2	0.8±0.1	80±0.7	Pecharroman et al., 1999
α	$^{[6]}$Al	104.3	2.4±0.2	0	16.0±0.2	This work
		130.32	2.38±0.5	0	14±1	Kraus et al., 1996
		78.172	2.4±0.0031	0.05±0.001	16±0.48	Sabarinathan et al., 2010
		104.23	2.38±0.01	0+0.03	16±0.2	Skibsted et al., 1991
		104.23	2.38	0	13.5	O'Dell et al., 2007
		182.4	2.5±1	0	14±2	Hagaman et al., 2010

This is a preprint, the final version is subject to change, of the American Mineralogist (MSA)
Cite as Authors (Year) Title. American Mineralogist, in press.
(DOI will not work until issue is live.) DOI: http://dx.doi.org/10.2138/am.2013.4364

Table 2. ^{27}Al NMR parameters for simulation of ^{27}Al NMR spectra. δ_{iso} is the isotropic chemical shift, C_q is the quadrupolar coupling constant, η is the asymmetry parameter. The $\Delta\delta_{iso}$ is the full width at half-maximum of the distribution of the isotropic chemical shift in the Czjzek model, which is used for simulation of the $^{[4]}$Al and $^{[6]}$Al peaks for (γ, δ)-Al_2O_3. The $^{[4]}$Al:$^{[6]}$Al ratio in ideal γ-, δ-, θ- and α-Al_2O_3 is 25:75, 38:62, 50:50, and 0: 100, respectively (Pecharroman et al., 1999; Repelin and Husson, 1990).

Sample	Phase	Al Site	δ_{iso} (ppm)	$\Delta\delta_{iso}$ (ppm)	C_q (MHz)	η	$^{[n]}$Al/($^{[4]}$Al+$^{[6]}$Al) ×100 (%)
27 nm	(γ, δ)	$^{[4]}$Al	72.5±1	10±3	5.70±1*	-	32±3
		$^{[6]}$Al	14.0±1	6.5±2.5	4.40±1*	-	68±3
	θ	$^{[4]}$Al	80.5±0.3	-	6.00±0.2	0.7±0.1	52±3
		$^{[6]}$Al	10.5±0.3	-	3.45±0.2	0	48±3
	α	$^{[6]}$Al	15.9±0.2	-	2.40±0.1	0	100
19 nm	(γ, δ)	$^{[4]}$Al	73.0±1	10±3	5.70±1.0*	-	30±3
		$^{[6]}$Al	14.0±1	6.5±2.5	4.50±1.0*	-	70±3
	θ	$^{[4]}$Al	80.5±0.3	-	6.00±0.2	0.7±0.1	51±3
		$^{[6]}$Al	10.5±0.3	-	3.45±0.2	0	49±3
	α	$^{[6]}$Al	16±±0.2	-	2.40±0.1	0	100
15 nm	(γ, δ)	$^{[4]}$Al	72.5±1	10±3	5.70±1.0*	-	26±3
		$^{[6]}$Al	14.0±1	6.5±2.5	4.50±1.0*	-	74±3
	θ	$^{[4]}$Al	80.5±0.3	-	6.00±0.2	0.7±0.1	51±3
		$^{[6]}$Al	10.5±0.3	-	3.45±0.2	0	49±3
	α	$^{[6]}$Al	15.9±0.2	-	2.40±0.1	0	100
Standard γ-Al_2O_3	γ	$^{[4]}$Al	72.5±1	10±3	5.70±1.0*	-	32±3
		$^{[6]}$Al	14.0±1	6.5±2.5	4.60±1*	-	68±3

* The quadrupolar NMR parameters, such as ν_q, η and σ are correlated among each other. The relations among them can be described with the following equation (de Lacaillerie et al., 2008):

$$\left\langle C_q^2 \right\rangle = \left(\frac{2}{3} I(2I-1)\right)^2 \left\langle \upsilon_q^2 (1+\eta^2/3) \right\rangle = \left(\frac{2}{3} I(2I-1)\right)^2 5\sigma^2$$

This is a preprint, the final version is subject to change, of the American Mineralogist (MSA)
Cite as Authors (Year) Title. American Mineralogist, in press.
(DOI will not work until issue is live.) DOI: http://dx.doi.org/10.2138/am.2013.4364 7/11

631 In Dmfit program (version released in 2011) used in the current study, therefore, C_q is u sed as
632 an input parameter and the σ value is automatically adjusted depending on C_q value: the
633 estimated σ is ~380±60 kHz and 280±50 kHz for $^{[4]}$Al and $^{[6]}$Al sites in (γ, δ)-Al_2O_3, respectively.
634
635 † The Gaussian or Lorentzian broadening factor (~300Hz to 2000 Hz) is applied to simulate Al
636 sites in (γ, δ)-, θ-Al_2O_3 and α-Al_2O_3, respectively.

This is a preprint, the final version is subject to change, of the American Mineralogist (MSA)
Cite as Authors (Year) Title. American Mineralogist, in press.
(DOI will not work until issue is live.) DOI: http://dx.doi.org/10.2138/am.2013.4364

Figure captions

Figure 1. Crystal structure of (A) γ-Al_2O_3, (B) θ-Al_2O_3, and (C) α-Al_2O_3 with crystallographically distinctive aluminum sites.

Figure 2. TEM images of (A) 27 nm, (B) 19 nm, and (C) 15 nm alumina nanoparticles before and after annealing at various temperatures.

Figure 3. XRD patterns for γ-Al_2O_3 and alumina nanoparticles. Red, blue, and purple vertical lines correspond to the peak positions and intensities of γ-Al_2O_3 (JCPDS file no.00-050-0741), δ-Al_2O_3 (JCPDS file no.00-016-0394), and θ-Al_2O_3 (JCPDS file no.00-23-1009), respectively.

Figure 4. (A) ^{27}Al MAS NMR spectra at 11.7 T for as-received alumina nanoparticles with varying particle size. (B) ^{27}Al MAS NMR spectra for 27 nm alumina nanoparticles at various magnetic fields.

Figure 5. ^{27}Al MAS NMR spectra at 11.7 T for (A) 27 nm, (B) 19 nm, and (C) 15 nm alumina nanoparticles with increasing annealing temperature up to 1573 K. (D) Comparison of $^{[6]}$Al peaks in ^{27}Al MAS NMR spectra for alumina nanoparticles with varying particle size.

Figure 6. Simulation of ^{27}Al MAS NMR spectra for as-received 27 nm alumina nanoparticles at 9.4, 11.7, and 14.1 T and for γ-Al_2O_3 at 11.7 T.

This is a preprint, the final version is subject to change, of the American Mineralogist (MSA)
Cite as Authors (Year) Title. American Mineralogist, in press.
(DOI will not work until issue is live.) DOI: http://dx.doi.org/10.2138/am.2013.4364

662 **Figure 7.** Simulation of ^{27}Al MAS NMR spectra at 11.7 T for (A) 27 nm, (B) 19 nm, and (C) 15
663 nm alumina nanoparticles with increasing annealing temperature.
664
665 **Figure 8.** Variation in populations of (γ, δ)-, θ-, and α-Al_2O_3 in (A) 27 nm, (B) 19 nm, and (C) 15
666 nm alumina nanoparticles with increasing annealing temperature up to 1573 K. (D–F)
667 show enlarged plots of Figure 8A–C at temperatures of 1400 and 1600 K.
668
669 **Figure 9.** ^{27}Al 3QMAS NMR spectra for 27 nm alumina nanoparticles (A) as-received and (B)
670 annealed at 1497 K for 2 h. (C) Expected center of gravity for γ-, δ-, θ-, and α-Al_2O_3
671 calculated on the basis of previous works: solid square (Kraus et al., 1996); solid
672 triangle (Perander et al., 2007); solid circle (Hagaman et al., 2010); solid diamond
673 (O'Dell et al., 2007); open circle (Sabarinathan et al., 2010); open diamond (Skibsted et
674 al., 1991); open square (Pecharroman et al., 1999). Red, blue, and purple symbols refer
675 to (γ, δ)-, θ-, and α-Al_2O_3, respectively.
676
677 **Figure 10.** ^{27}Al 3QMAS NMR spectra for 15, 19, and 27 nm alumina nanoparticles after
678 annealing at various temperatures.
679
680 **Figure 11.** Normalized variation in the (A) (γ, δ)- and θ- Al_2O_3, (B) α-Al_2O_3 population in
681 particles of several sizes annealed at several temperatures.
682
683
684
685

This is a preprint, the final version is subject to change, of the American Mineralogist (MSA)
Cite as Authors (Year) Title. American Mineralogist, in press.
(DOI will not work until issue is live.) DOI: http://dx.doi.org/10.2138/am.2013.4364

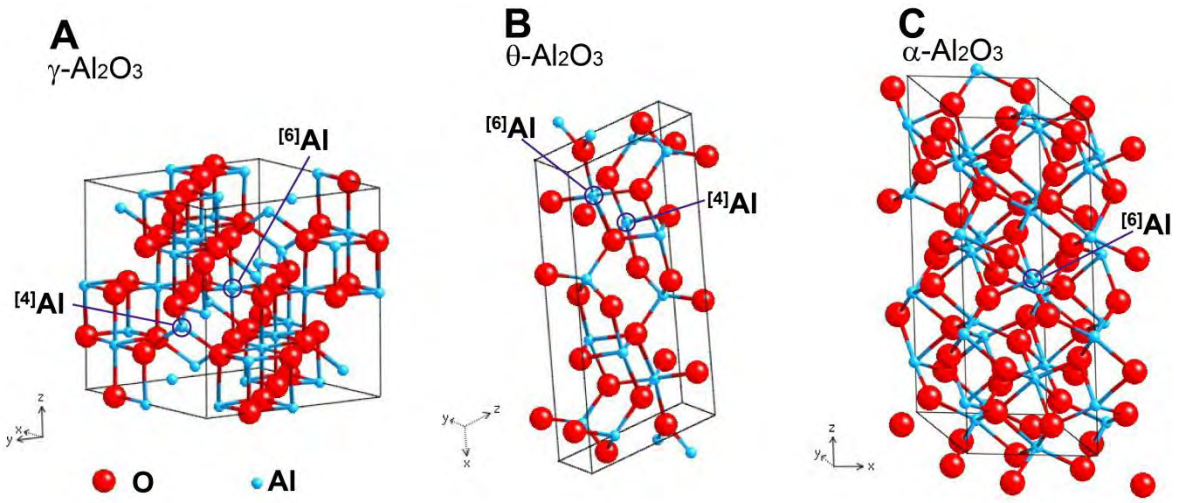

Figure 1

This is a preprint, the final version is subject to change, of the American Mineralogist (MSA)
Cite as Authors (Year) Title. American Mineralogist, in press.
(DOI will not work until issue is live.) DOI: http://dx.doi.org/10.2138/am.2013.4364

698

699

700

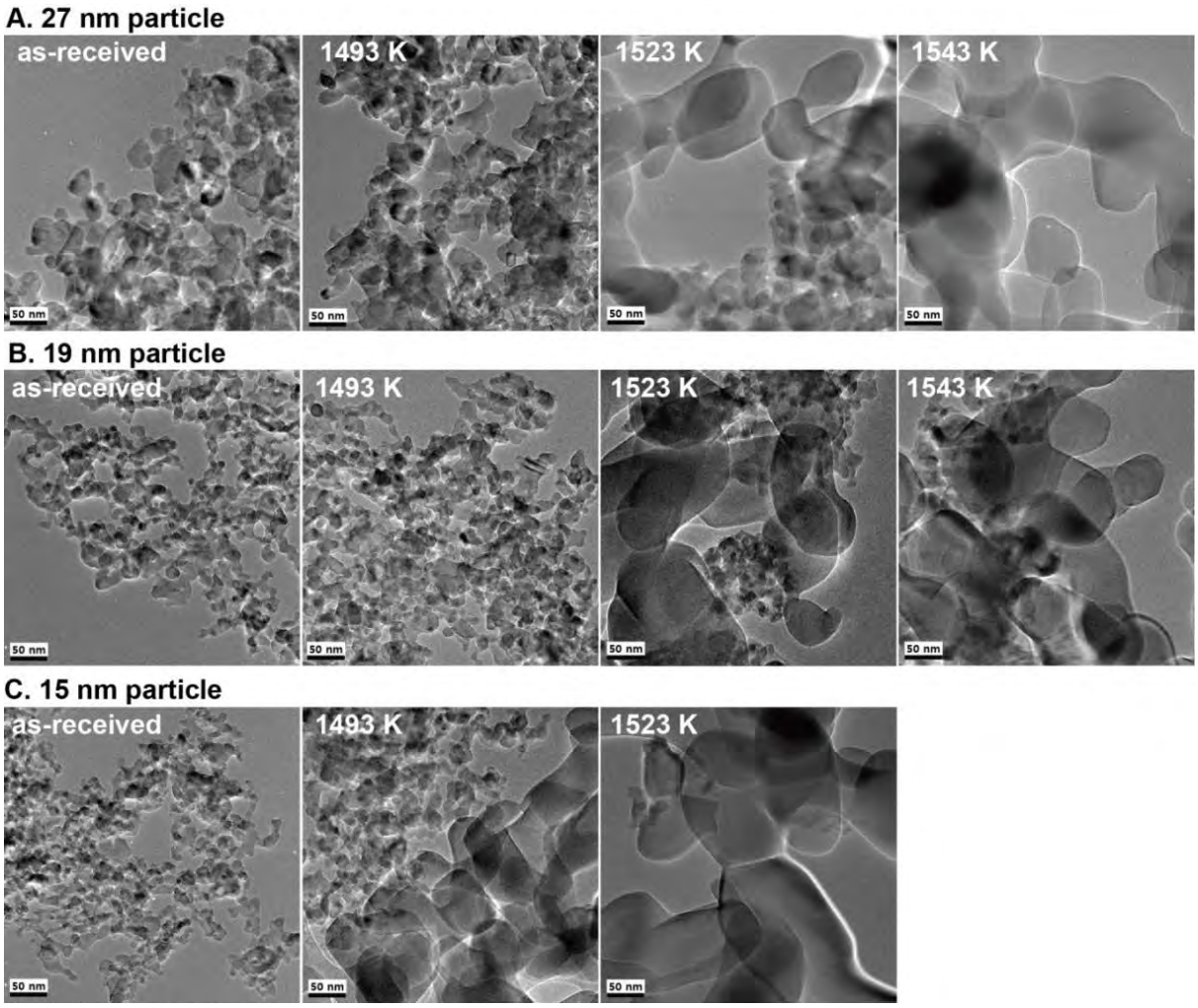

701

702 **Figure 2**

703

704

This is a preprint, the final version is subject to change, of the American Mineralogist (MSA)
Cite as Authors (Year) Title. American Mineralogist, in press.
(DOI will not work until issue is live.) DOI: http://dx.doi.org/10.2138/am.2013.4364

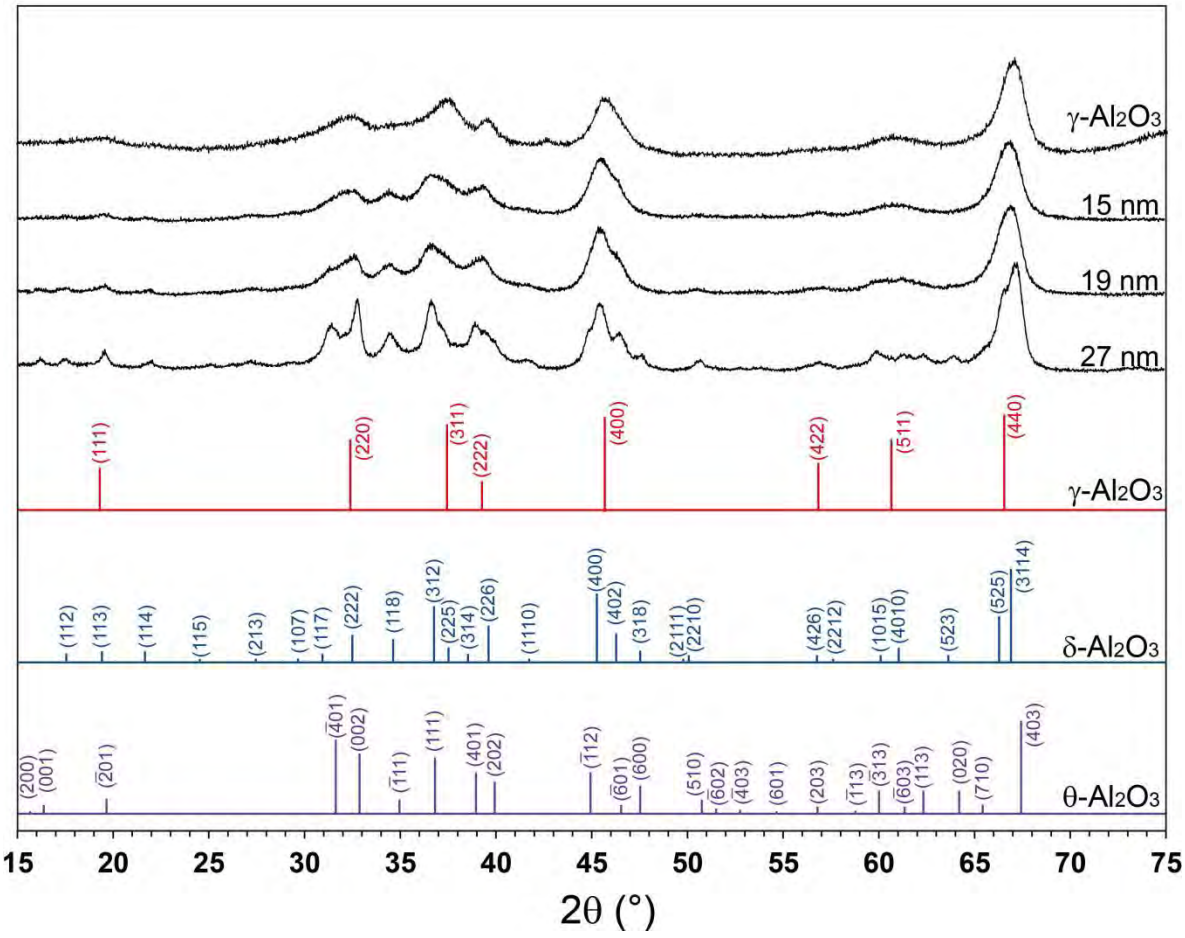

Figure 3

This is a preprint, the final version is subject to change, of the American Mineralogist (MSA)
Cite as Authors (Year) Title. American Mineralogist, in press.
(DOI will not work until issue is live.) DOI: http://dx.doi.org/10.2138/am.2013.4364

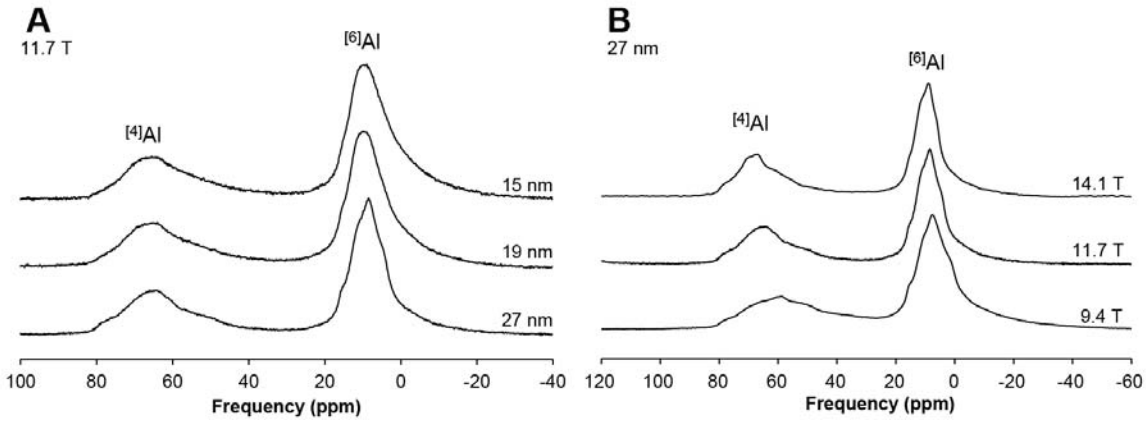

Figure 4

This is a preprint, the final version is subject to change, of the American Mineralogist (MSA)
Cite as Authors (Year) Title. American Mineralogist, in press.
(DOI will not work until issue is live.) DOI: http://dx.doi.org/10.2138/am.2013.4364

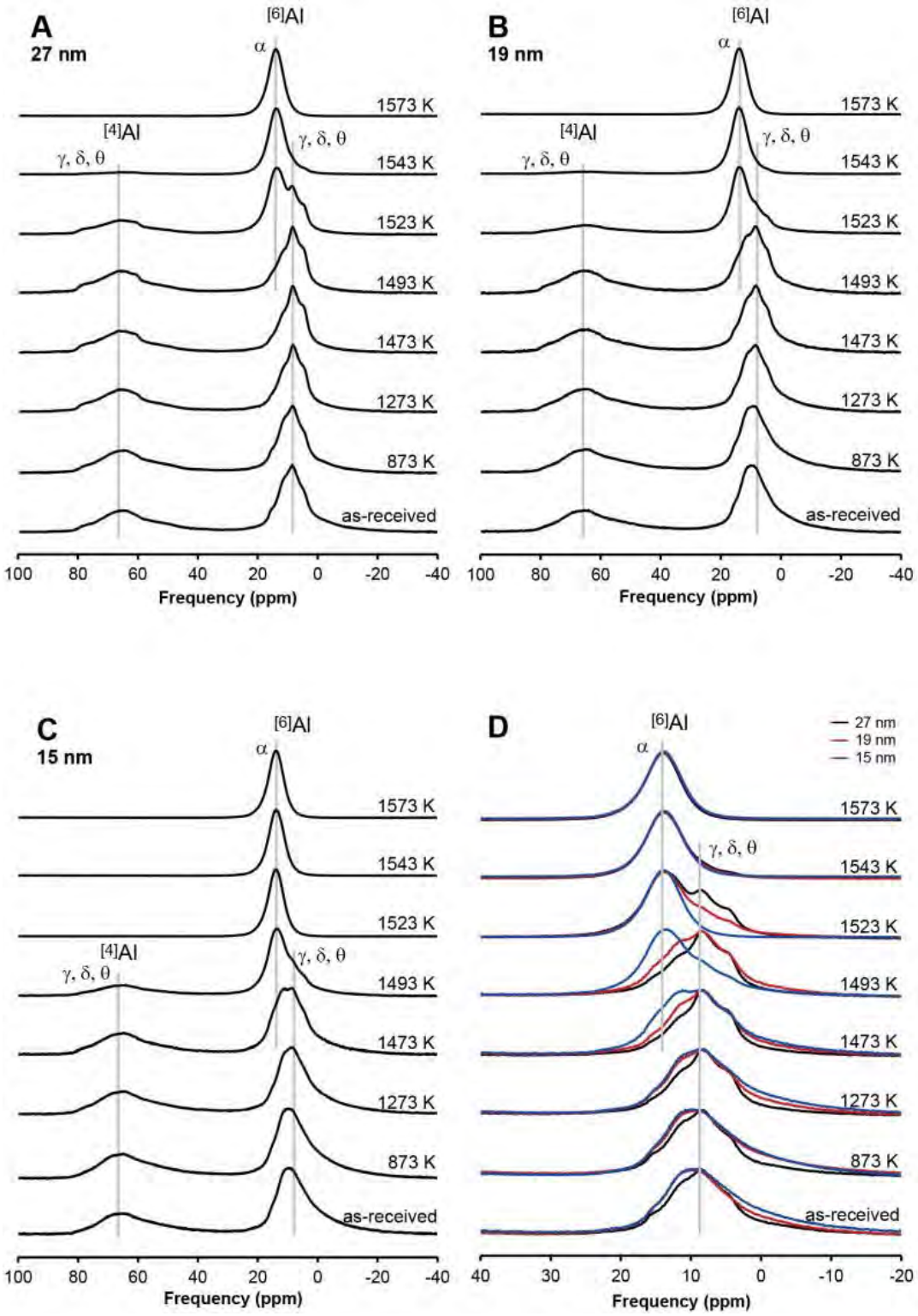

Figure 5

This is a preprint, the final version is subject to change, of the American Mineralogist (MSA)
Cite as Authors (Year) Title. American Mineralogist, in press.
(DOI will not work until issue is live.) DOI: http://dx.doi.org/10.2138/am.2013.4364

727

728

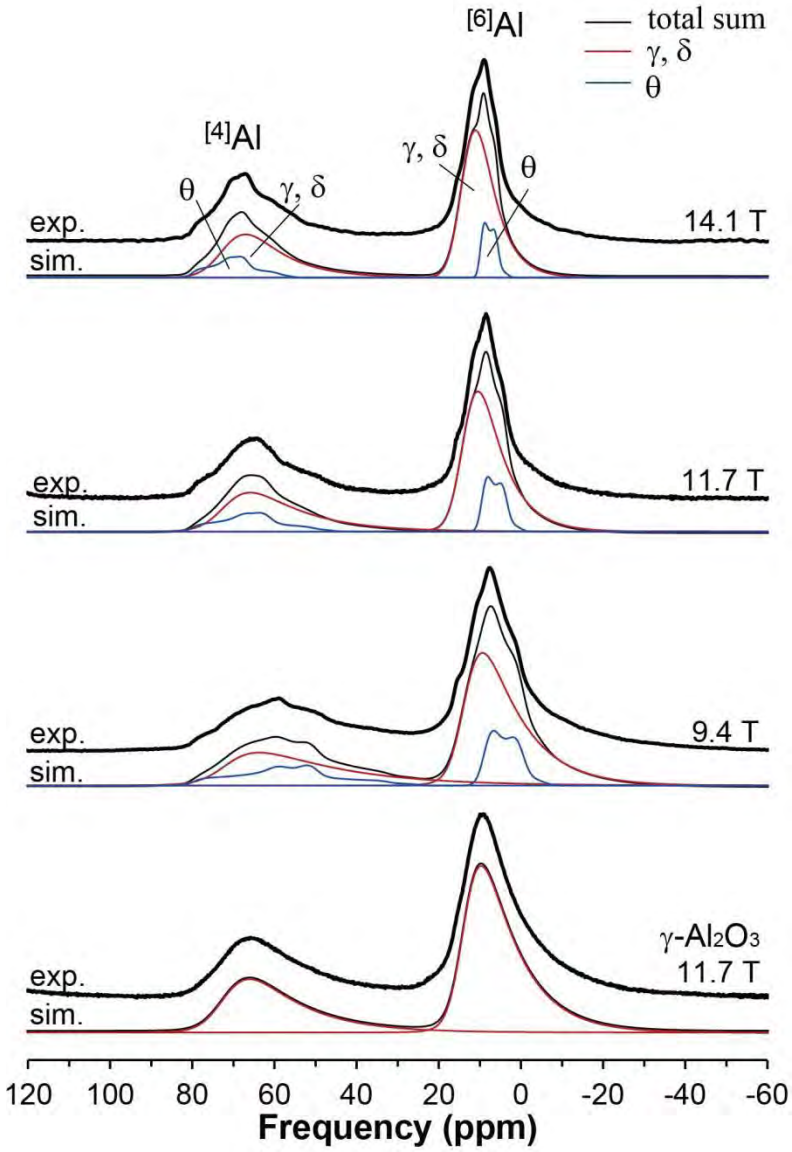

729

730 **Figure 6**

This is a preprint, the final version is subject to change, of the American Mineralogist (MSA)
Cite as Authors (Year) Title. American Mineralogist, in press.
(DOI will not work until issue is live.) DOI: http://dx.doi.org/10.2138/am.2013.4364

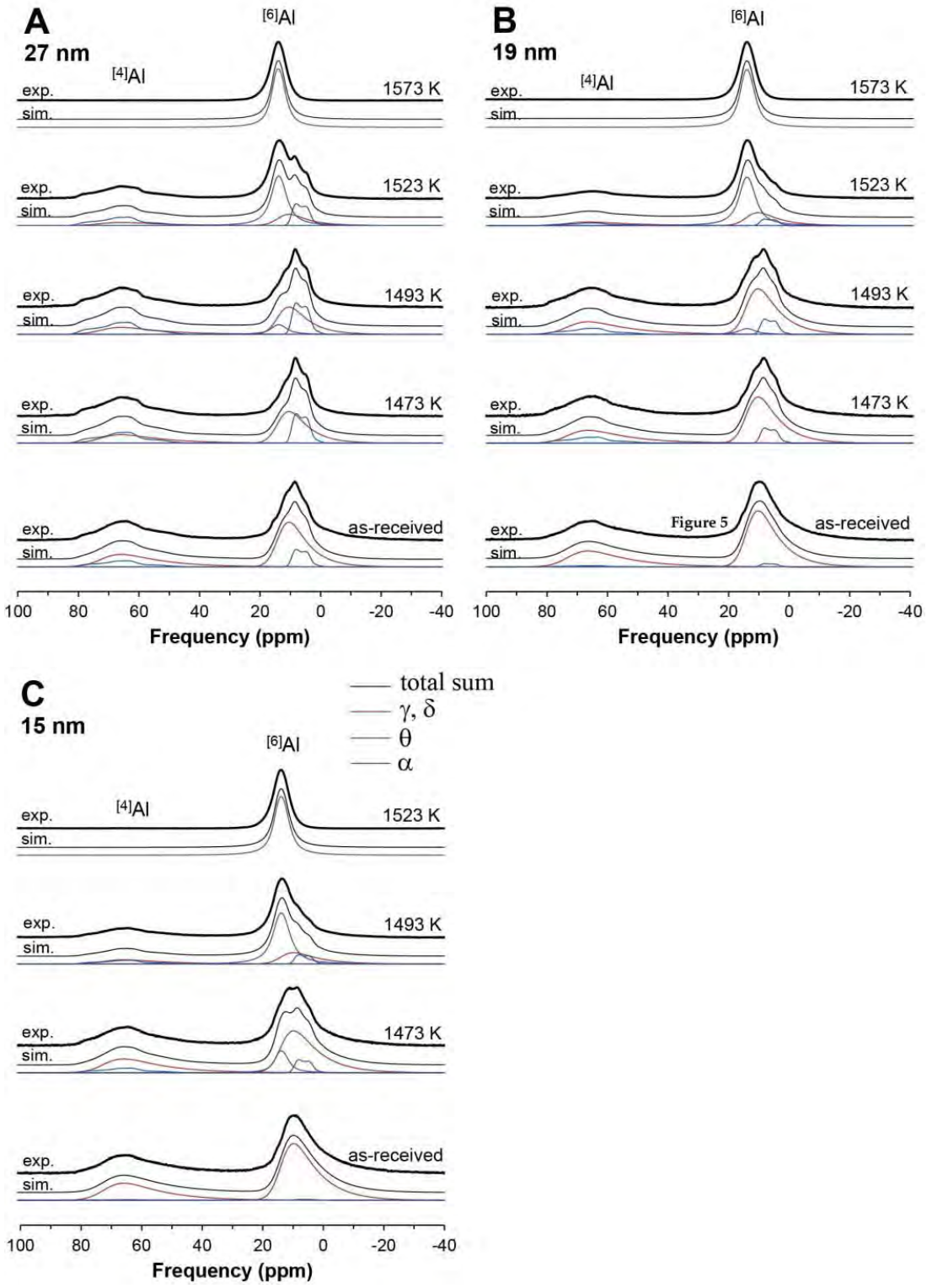

731

732 **Figure 7**

This is a preprint, the final version is subject to change, of the American Mineralogist (MSA)
Cite as Authors (Year) Title. American Mineralogist, in press.
(DOI will not work until issue is live.) DOI: http://dx.doi.org/10.2138/am.2013.4364

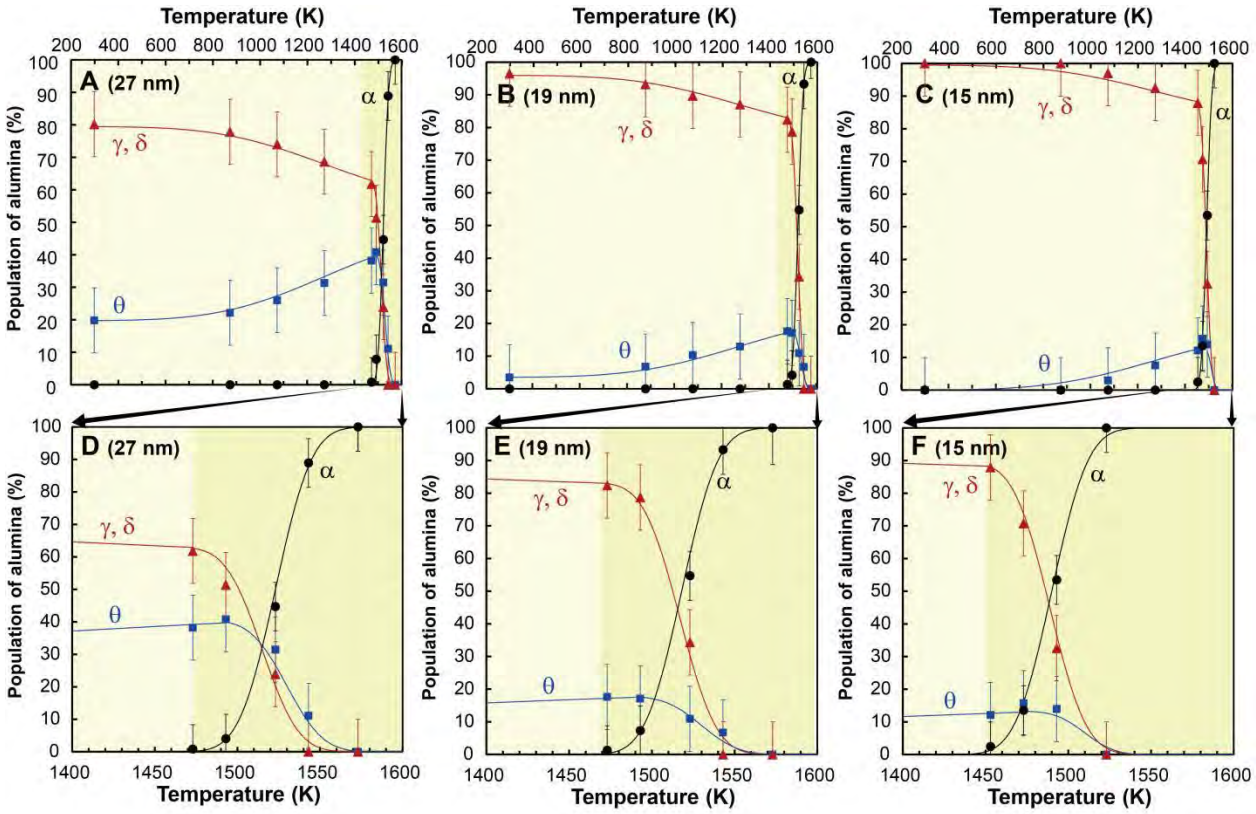

Figure 8

This is a preprint, the final version is subject to change, of the American Mineralogist (MSA)
Cite as Authors (Year) Title. American Mineralogist, in press.
(DOI will not work until issue is live.) DOI: http://dx.doi.org/10.2138/am.2013.4364

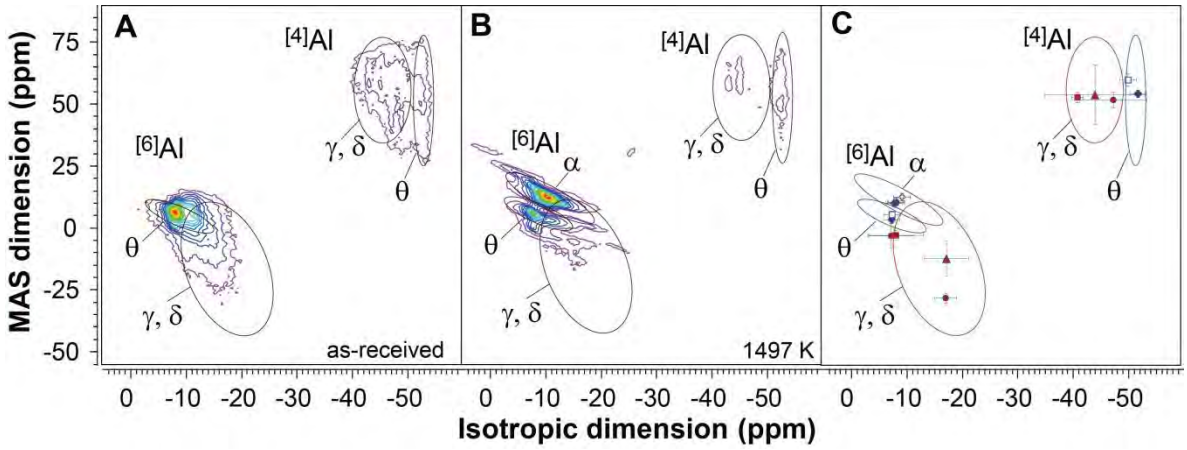

Figure 9

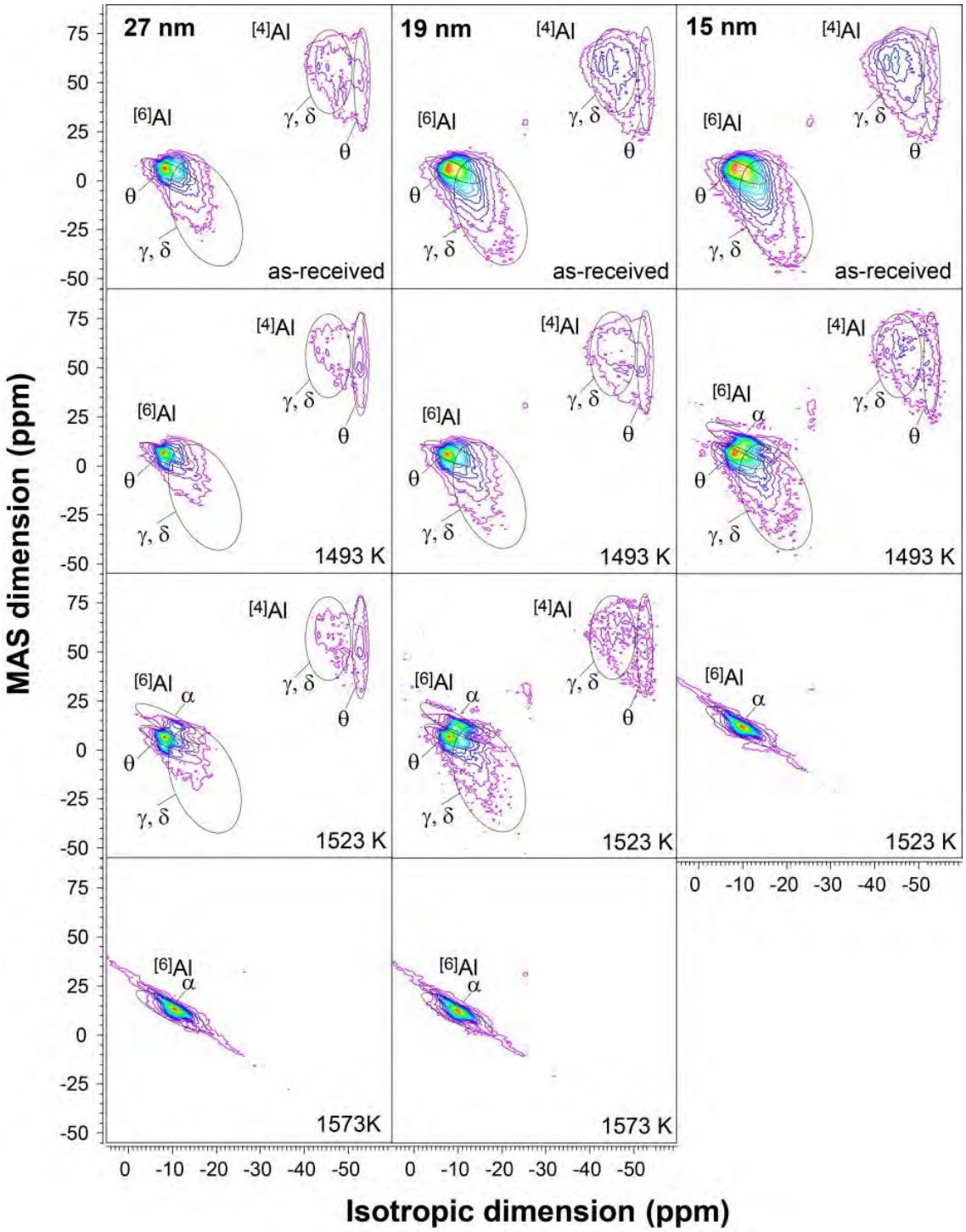

Figure 10

This is a preprint, the final version is subject to change, of the American Mineralogist (MSA)
Cite as Authors (Year) Title. American Mineralogist, in press.
(DOI will not work until issue is live.) DOI: http://dx.doi.org/10.2138/am.2013.4364

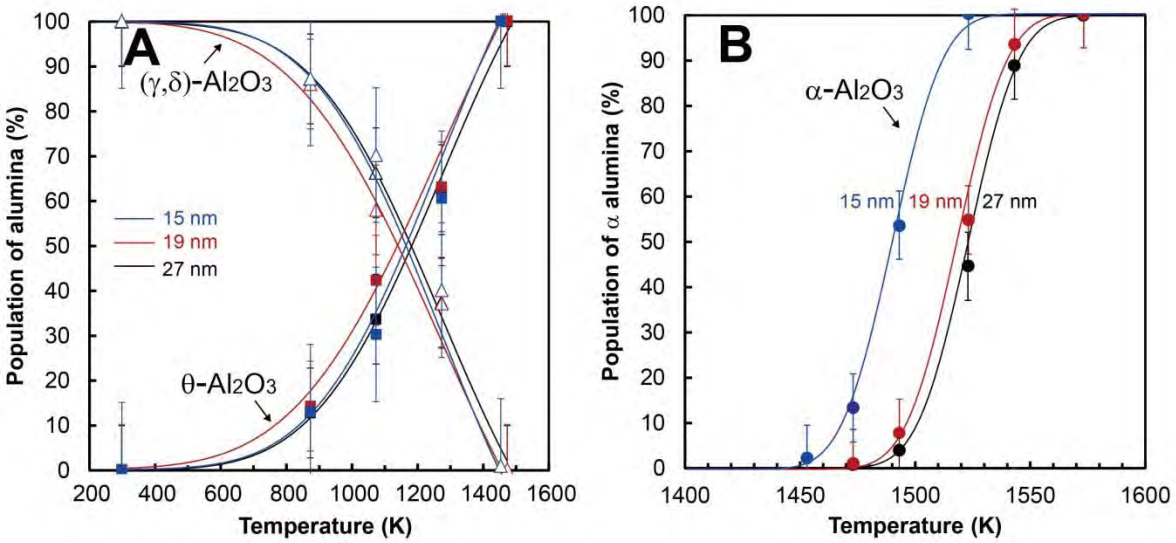

Figure 11

This is a preprint, the final version is subject to change, of the American Mineralogist (MSA)
Cite as Authors (Year) Title. American Mineralogist, in press.
(DOI will not work until issue is live.) DOI: http://dx.doi.org/10.2138/am.2013.4364

Supporting Materials

We present the complete set of ^{27}Al MAS NMR spectra, which is not shown in the manuscript. Figure S1 presents the simulated ^{27}Al MAS NMR spectra for alumina nanoparticles with varying particle size and annealing temperature up to 1573 K.

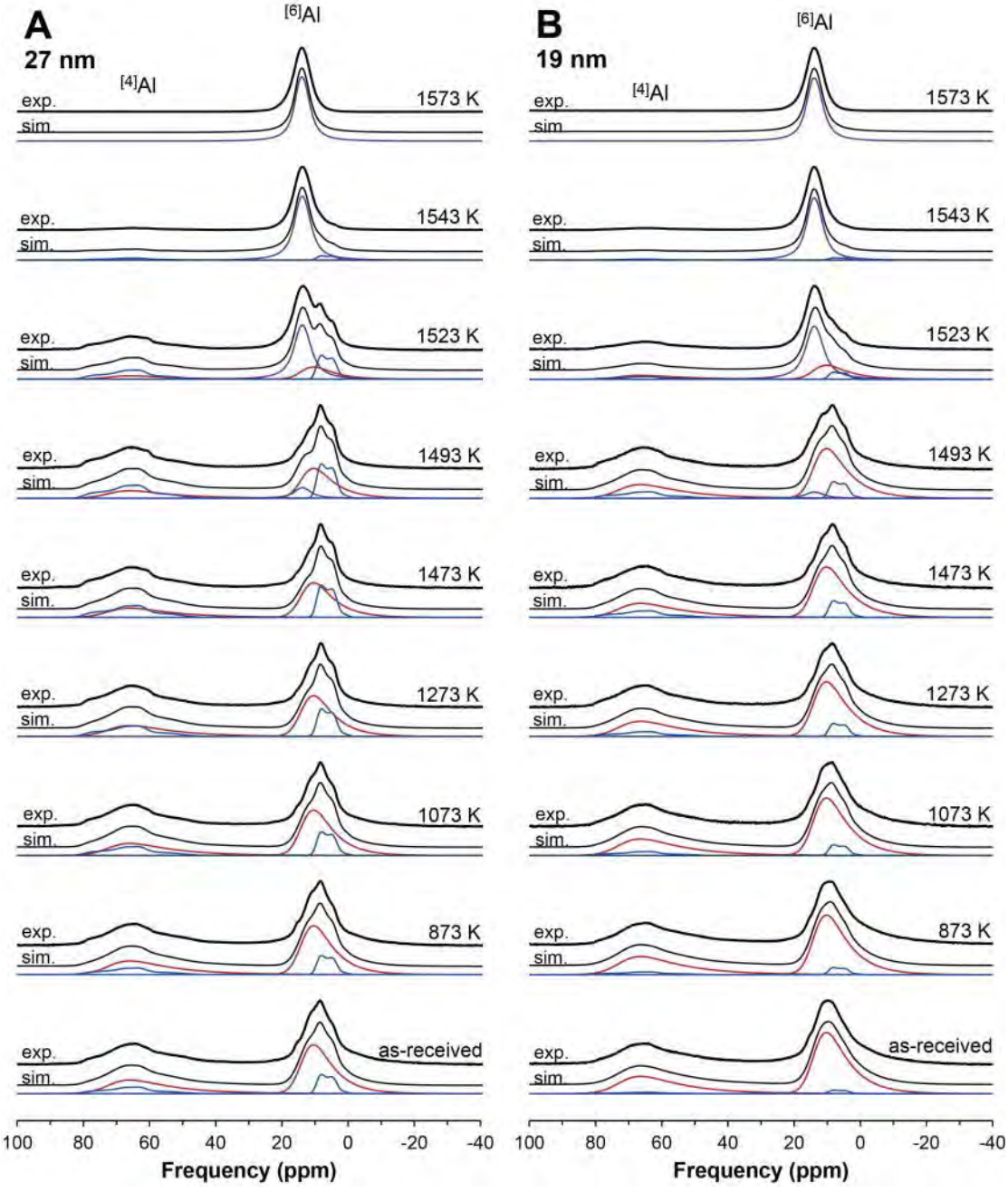

This is a preprint, the final version is subject to change, of the American Mineralogist (MSA)
Cite as Authors (Year) Title. American Mineralogist, in press.
(DOI will not work until issue is live.) DOI: http://dx.doi.org/10.2138/am.2013.4364

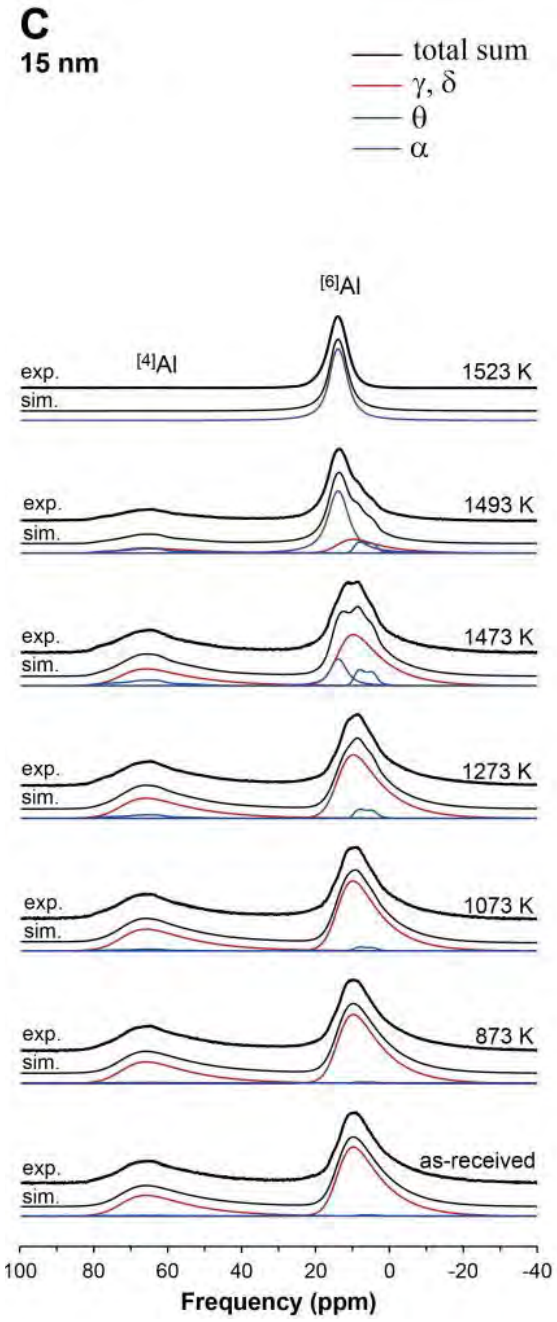

775

776 **Figure S1.** Simulation of ^{27}Al MAS NMR spectra at 11.7 T for (A) 27 nm, (B) 19 nm, and (C) 15

777 nm alumina nanoparticles with increasing annealing temperature.

778

779

This is a preprint, the final version is subject to change, of the American Mineralogist (MSA)
Cite as Authors (Year) Title. American Mineralogist, in press.
(DOI will not work until issue is live.) DOI: http://dx.doi.org/10.2138/am.2013.4364

780 Figure S2 presents the ^{27}Al 3QMAS NMR spectra for alumina nanoparticles with
781 varying particle size and annealing temperature.
782

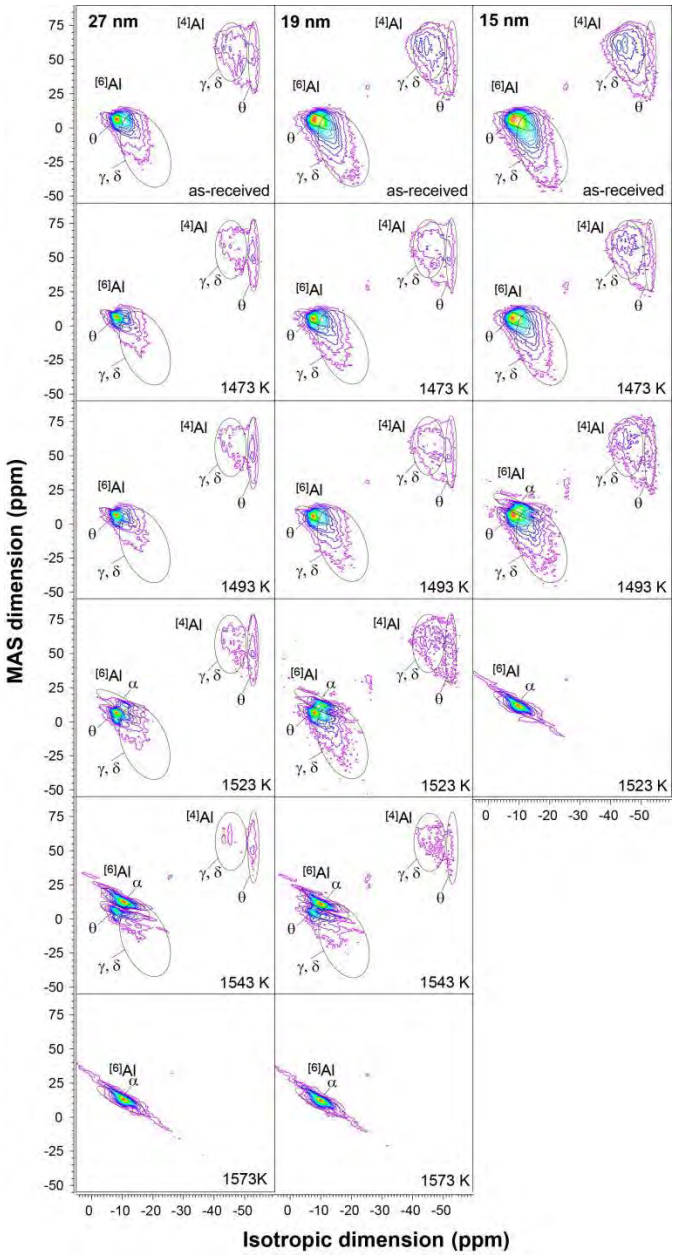

783

784 **Figure S2.** ^{27}Al 3QMAS NMR spectra for 15, 19, and 27 nm alumina nanoparticles with
785 increasing annealing temperature.